Ceramics International 47 (2021) 14862–14878

Contents lists available at ScienceDirect

Ceramics International

journal homepage: www.elsevier.com/locate/ceramint

Utilization of green reductant Thuja Orientalis for reduction of GO to RGO

Pushpendra Kumar [a,*], Harish [a], Gunther Andersson [b], Kiran M. Subhedar [c], Hoshiyar S. Dhami [d], Gunjan Gupta [e], Anoop K. Mukhopadhyay [a], Rajendra P. Joshi [f,**]

[a] Department of Physics, Manipal University Jaipur, Jaipur-303007, Rajasthan, India
[b] College of Science and Engineering, Flinders University, Adelaide, SA, 5001, Australia
[c] Advanced Carbon Products, Division of Advanced Materials and Devices, Academy of Scientific and Innovative Research (AcSIR)-NPL, CSIR-National Physical Laboratory (NPL), New Delhi, 700012, India
[d] Uttarakhand Residential University, Almora, 263601, Uttarakhand, India
[e] RI Nanotech India, Sector IIDC, Rudrapur, 263153, India
[f] RI Instruments and Innovation India, Haldwani, 263139, Uttarakhand, India

ARTICLE INFO

Keywords:
Graphene
Green reductant
Thuja orientalis
Alpha tocopherol
GCMS
Raman spectroscopy

ABSTRACT

It is well known that graphene (G), graphene oxide (GO) and reduced graphene oxides (RGO) are materials of today with immense application potentials. However, to realize the same large scale, reproducible, sustainable synthesis techniques such as greener methods which avoid utilization of toxic chemicals for synthesis, must be adopted. It is in this context, that here we report the reduction of GO to RGO by the extract of Thuja Orientalis (TO) seeds. As such, TO is a well-known bio-resource for medicinal and various other biotechnological applications as it contains Alpha Tocopherol, the major constituent of vitamin E. To the best of our knowledge, despite the wealth of literature, the current work makes a pioneering effort in applying TO seeds extract for reduction of GO to RGO. Thus, the reduction of GO, synthesized by the well-known modified Hummer's method to RGO by TO extract, is confirmed from the results obtained by ultra-violet visible (UV–Vis) spectroscopy, Fourier transform infrared (FTIR) spectroscopy, transmission electron microscopy (TEM), high resolution transmission electron microscopy (HRTEM), energy dispersive X-ray (EDX) analysis, selected area electron diffraction (SAED), Raman spectroscopy, X-ray photoelectron spectroscopy (XPS), X-ray diffraction (XRD), atomic force microscopy (AFM) and especially, gas chromatograph mass spectrometry (GCMS) techniques. Furthermore, the GCMS study is used to identify the compound Alpha Tocopherol responsible for reduction of GO to RGO. Based on current experimental evidences and literature views, the possible mechanism of reduction is suggested. Finally, the implications of present studies in the perspective of large scale, sustainable synthesis of RGO for various technological applications are discussed.

1. Introduction

Graphene (G), graphene oxide (GO) and reduced graphene oxides (RGO) are materials evolving today more than yesterday both in terms of basic science and application perspective [1–3]. They provide a unique combination of electrical, optical, mechanical, thermal as well as biocompatibility and biotechnological properties [3–9]. Hence, they continue to foster a wide range of research interests [1–9]. Graphene is synthesized usually by the "Tape" method [10], chemical vapor deposition (CVD) [11], hydrothermal method [12], supercritical fluid processing [13] and of course, chemical exfoliation [14]. The most well-known Hummer's method [15,16] produces a water-soluble GO obtained by controlled oxidation of graphite. Subsequently, GO is chemically reduced to get RGO [17]. A significant amount of recent research is devoted to GO and GO-composites for supercapacitor [18], sensor [19] and intercalation applications [20]. RGO and RGO-composites enjoy today even further enhanced research focus mainly due to their importance for energy storage [21], energy production e.g., proton exchange membrane (PEM) fuel cells [22], anodes of Li-ion batteries [23–25] and biomedical applications [26–30]. However, highly toxic and explosive chemical e.g., hydrazine used for the synthesis of GO *is not eco-friendly* [17] *and hence, is far from*

* Corresponding author.
** Corresponding author.
E-mail addresses: pushpendra.kumar@jaipur.manipal.edu (P. Kumar), rjoshinano@gmail.com (R.P. Joshi).

https://doi.org/10.1016/j.ceramint.2020.08.063
Received 22 April 2020; Received in revised form 7 August 2020; Accepted 8 August 2020
Available online 16 August 2020

recommended.

Therefore, the major focus for large scale production of RGO is now on plant extracts used as green reductants, Table 1 [29–49]. Accordingly, many mechanisms are suggestively proposed but the confirmation of GO to RGO synthesis is mostly done based on characterization results [29–49]. These mechanisms widely vary from each other and hence, these shall be discussed later in details. Other attempts to convert GO to RGO include use of metals (e.g., iron, zinc, aluminium and manganese) [50–53] and acids with various functional groups (e.g., oxalic acid, L-ascorbic acid, gallic acid, formic acid and caffeic acid) [54–58] as green reductants. Further, supercritical alcohols [13,59] as well as natural cellulose and sugars [60,61] are also used as green reductants. Furthermore, microbes [62–64] and many other vitamins e.g., vitamin C and organic resources [65–67] are also utilized as green reductants to obtain RGO. In addition, alkaline e.g., potassium hydroxide (KOH), sodium hydroxide (NaOH) [68], sodium bicarbonate (Na_2CO_3) [69] and sodium acetate ($C_2H_9NaO_5$) [70] solutions and numerous other materials also are reported [71] as green reductants to synthesize RGO. However, apart from the plant extracts these other green reductants also have their own problems. For instance, when metals are used to develop RGO there may be inevitable presence of impurities [50–53]. Again C/O ratios are relatively lower when gallic acid [57] or supercritical alcohols [59] are used. On the other hand, ionic liquid is needed for using cellulose [60] and relatively toxic alkaline atmosphere is required for using sugar [61] for reduction of GO to RGO. Thus, despite the wealth of literature [29–61] many such challenges are yet to be overcome as far as the green reductants are concerned. In this context, it is interesting to note from the literature survey presented above in Table 1 that, there has not been a single attempt yet to use the extract of TO seeds for synthesis of RGO.

It is already well-known [72] that TO contains essential oils. These oils are traditionally used to treat fungus infections. Further, these oils or their derivatives are also used to treat cancer, moles and parasitic worms. The TO extract contains α-thujone. This is the component useful as an insecticide agent. In addition, α-thujone acts as an anti-helminthic agent for the treatment of parasitic worms [73]. Most importantly, the bio-technological potential of TO is well recognized for treatment of various critical disease. These include e.g., anti-proliferation treatment, anti-apostosis treatment, uterine cancer treatment, cystitis treatment, rheumatism treatment, amenorrhea treatment, psoriasis treatment, enuresis treatment and bronchial catarrh treatment [74–76]. Antioxidant properties of TO are also well established [77]. Further, the ethanol fraction of TO exhibits excellent hepato-protective quality [78]. The basis of such unique quality of TO extract is the presence of vitamin E which has Alpha Tocopherol as the major component [79–84]. It is interesting to note further that Alpha Tocopherol is most potent natural antioxidant with the highest capacity to scavenge reactive oxygen species (ROS). Therefore, it has high therapeutic potential for life threating diseases like cardiovascular failure, cancer and Alzheimer's disease [85]. Furthermore, recent works exhibit that TO extract is also a very important bio-resource for synthesis of Ag nanoparticles (NPs) [86,87]. The aforesaid facts establish the genesis of TO as the material of choice in the present work.

Since there has not been a single attempt yet to use the extract of TO seeds for synthesis of RGO; this is the major, novel objective of the present work. But this is not the only novelty of the present work. The major novelty lies in the fact that TO contains Alpha Tocopherol, a natural antioxidant; as mentioned above. Thus, the major novelty of present work lies in application of Alpha Tocopherol present in TO seeds extract. In other words, the major objective of the present work is to utilize the antioxidant property of Alpha Tocopherol present in TO seeds extract for reduction of GO to RGO. The samples obtained from these experiments are characterized by UV–Vis spectroscopy, FTIR spectroscopy, TEM, HRTEM, EDX analysis, SAED, Raman spectroscopy, XPS, XRD, AFM and especially, the GCMS techniques. The results derived from these characterization experiments confirm beyond any doubt that the presence of this special reducing agent e.g., the extract of TO seeds can successfully produce RGO and few layer RGO sheets in aqueous solution. Finally, the possible mechanisms are also suggested based on existing knowledgebase.

2. Materials and methods

2.1. Materials

2.1.1. Synthesis of GO

At first the graphite powder (Sigma –Aldrich, USA) mixed with appropriate quantities of sulfuric acid, potassium per-sulphate and phosphorus pentoxide (Sigma –Aldrich, USA) was kept for 6 h at 80 °C and then cooled down to room temperature. Then, it was diluted with 200 ml deionized (DI) water (Millipore Direct Q 3UV, France). To remove residual acid, the mixture was filtered and washed several times with DI water. Thus, the residue obtained was dried. This was the pre-oxidized graphite powder which was subsequently converted to GO using the well-known Hummer's method [15,16]. Briefly, the pre-oxidized graphite powder was mixed with the appropriate quantity of sulfuric acid at 80 °C followed by very slow addition of potassium permanganate with continuous, vigorous stirring while kept in ice bath. After continuous, vigorous stirring for 2 h at 35 °C, DI water was added to the mixture. Finally, the reaction was terminated with addition of further DI water and hydrogen peroxide. After filtering the mixture, it was washed with dilute hydrochloric acid to remove the metal ions. Repeated washing with DI water and centrifugation of the yellow brown residue was continued until pH of rinsed water became close to 7, the pH of neutral water. This yellow brown residue was the GO material [15,16].

2.1.2. Synthesis of RGO

First, the procured TO seeds were naturally dried for about 10 days. It was done in the ambient laboratory atmosphere at room temperature. The dried seeds were mechanically ground. This step gave the TO powders. Then, about 1.5 g TO powder mixed with 45 ml ethanol was stirred for 4 h in a magnetic stirrer, followed by ultrasonication to ensure proper extraction. The extract of TO was then filtered with micro syringe filter. Prepared GO was reduced to RGO by using this freshly prepared extract of TO. To remove excess reductant from RGO solution; the repeated centrifugation with DI water was done [29].

Almost parallelly, 100 mg of GO powder mixed with 100 ml DI water was ultrasonicated for 1 h to disperse the GO sheets in water. Now, 25 ml of fresh TO extract was mixed with 100 ml of the freshly prepared GO solution. After 6 h, the yellow brown GO was reduced to completely dark RGO. Finally, 2 g of graphite converted to 1.4 g RGO with a process yield of ~70%.

2.2. Characterization

2.2.1. UV–Vis and FTIR spectroscopy

The wavelength range from 200 to 1100 nm was scanned to measure the absorbance spectra of both GO and RGO using a spectrophotometer (Lambda 950, PerkinElmer, USA). Similarly, the FTIR spectra of the GO and RGO materials were measured in the range of wavenumber 400–4500 cm^{-1} using a FTIR spectrometer (Nicolet 6700, Thermo Scientific, USA) with a resolution of <0.001 cm^{-1} and spectroscopic grade KBr (≥99.99%, Fisher Scientific, USA) pellet made in a die (PCI, India) as the internal reference standard. The background was collected for the DI water after mounting it in cell holder in FTIR spectrometer. An amount of ~5 μl each of both the GO and the RGO solutions in DI water were kept one by one in desiccators equipped with silica bag to record the respective spectrum. This step was followed by subtraction of water peaks by water correction option of OMNIC software available in the FTIR machine.

Table 1
Literature survey on green, plant-based reductants and corresponding mechanisms for reduction of GO to RGO.

Reducing agent	Reduction conditions	GO to RGO reduction proven by main experimental techniques (*)	Suggested mechanisms	Ref. No.
Emblica officinalis (EO)	Extract of EO fruit added to GO suspension, reflux 1h, followed by heating for 24 h at 90 °C	XRD, FTIR,UV–Vis, SEM, HRTEM, PL	Reductant rolesof vitamin C,flavonoids andmany othercompounds.	[29]
Tagetes erecta flower extract	100 ml of flower extract was added to $Cu(NO_3)_2$-RGO solution and stirred for 3 h at 95 °C	XRD, FTIR,UV–Vis, SEM, HRTEM	Phytochemicals and antioxidants present in flower extract	[30]
Marigold flower extract	5 ml of marigold flower extract added to 20 ml GO suspension and stirred for 3 h at 95 °C	XRD, FTIR,UV–Vis, SEM,	Phytochemicals	[31]
Clove oil extract	Clove extract mixed with 75 g GO suspension in 50 ml DW and refluxed for 50 min	XRD, FTIR,UV–Vis, SEM, TEM, PL	Antioxidants present in clove oil extract	[32]
Beta carotene	Beta carotene Extract mixed with 2 $mg.ml^{-1}$GO suspension at 95 °C for 24 h	UV–Vis, XRD, TEM, FTIR, TGA,Raman	Oxygen anions reactwith the epoxide moiety of GO leading to creation of aldehydes and removal of one water molecule	[33]
Green carrot root	Carrot root extract mixed with 0.5 mg ml^{-1} suspension at room temperature (RT) for 48 h	XRD, FTIR, Raman,XPS, TEM,AFM, TGA	Endophytic micro-oragnisms present in green carrot toot	[34]
Curcumin	Curcumin seed extract mixed with GO suspension at 85 °C for 2 h	TEM, AFM,Raman, UV–Vis, AFM,TGA, DSC	Antioxidant action of polyphenols in curcumin seed extract	[35]
Grape juice	Grape juice mixed with 0.6 mg ml^{-1} GO suspension at 95 °C for 1, 3 and 6 h	UV–Vis, FTIR XRD, TEM	Antioxidant properties of polyphenols present in grape juice	[36]
Green tea polyphenol	Green tea solution mixed with 1 mg ml^{-1} GO suspension at 80 °C for 8 h	UV–Vis, Raman, XPS, TGA, XRD,	Antioxidant roles of polyphenols groups present in tea polyphenols	[37]
Green tea solution	50 mg GO added in the tea solution and sonicated for only 30 min, resultant colloid refluxed at 90 °C in a nitrogen atmosphere	UV–Vis, Micro-Raman, XPS, TGA, XRD, AFM, TEM, SEM	Antioxidant roles of multiple pyrogallol and catechol groups present in tea polyphenols	[38]
Green tea polyphenol and iron	Tea solution added to 0.1 mg ml^{-1} GO suspension at 40, 60 and 80 °C for 10 min	UV–Vis, Raman, AFM, SEM, TEM	Antioxidant activity of green tea polyphenol in presence of iron	[39]
Rose water	10 ml rose water (12%) mixed to (7 mg. ml^{-1}) 10 ml exfoliated GO suspension, ultrasonicated for 30 min and mixture heated for 5 h at 95 °C	UV–Vis, Raman, FTIR, AFM, SEM, TEM, XRD	Antioxidant activity of phenolic compounds plus flavonol glycosides	[40]
Coconut water	150 ml of fresh filtered tender coconut water added to 100 mg GO, 60 min sonication at RT followed by placement in an oil bath at 100 °C for 12, 24 and 36 h	UV–Vis, Raman, FTIR, AFM, SEM, TEM, XRD, Zeta potential	Reductant role of C. nucifera (cocos nucifera l)	[41]
Citrus sinensis peel, leaves of C.esculenta and M. ferrea linn	2 mg ml^{-1} GO suspension treated with corresponding phytoextracts at RT for 8–10 h followed by 5–8 h reflux	FTIR, UV–Vis, XRD, TGA, TEM,Raman, Electrical conductivity	Conversion of Phytochemicals to Quinones in presence of ROS and hence, reduction of oxygen containing groups present in GO	[42]
Spinach leaves	1.6 mg ml^{-1} GO suspension treated with extract of spinach and refluxed for 30 min at 100 °C.	XRD, UV–Vis, TEM	Roles of antioxidant phytochemicals such as vitamin C, acid derivatives of flavonoids and other compounds	[43]
Pomegranate	5 mg ml^{-1} GO in 400 mg ml^{-1} plant extract stirred for 8 h at 98 °C	XRD, FTIR,FT-Raman, UV–Vis, TGA, SEM, TEM, HPLC Fluorescence	Carbohydrates, glycosides, flavonoids, phytosterols, protein etc. are responsible for the reduction	[44]
Eucalyptus leaf extract	Leaf extract (10 g l^{-1}) and GO (0.5 g l^{-1}) solution of 1:4 for 8 h at 80 °C	UV–Vis, FTIR,SEM, TEM, GCMS	Reductant roles of many compounds such as eucalyptols, aldehydes, terpineols, amides etc.	[45]
U. dioica leaves	u. dioica powder added to GO suspension of 0.8 g l^{-1} stirrer for 1 h at 90 °C	FESEM, TEM,Raman	Reductant roles of many compounds e.g., fatty acids, carotenoids, polyphenols, histamines, phenolic acids, serotonins etc. present in the leaves, and histamine and serotonin containing NH_2 functional groups	[46]
Starch	0.5 mg starch in 1 ml GO, pH value adjusted by ammonia water, hydrothermally heated for 15 min at 120 °C	UV–Vis, DLS, Zeta potential,XRD, Raman XPS, TGA, TEM,ATR-IR	Interactions of GO with OH group of starch leads to degradation of starch to aldehydes and ketones	[47]
Tanin	Tanin extract solution (e.g., 400 wt% relative to GO) mixed with 1.1 mg ml^{-1} GO suspension sonicated for 30 min, reduction at 80 °C, 10 h	XPS, Raman,XRD, AFM, UV–Vis, TEM	Reductant characteristics of abundant catechol and pyrogallol present in tannins	[48]
Cinnamon extract	Cinnamon extract mixed with 1.6 mg ml^{-1} GO suspension by 40 min sonication and refluxed for 0.75 h	XRD, UV–Vis, TEM	Antioxidant and free radical scavenging activities of cinnamaldehyde, eugenol and their derivatives present in cinnamon bark	[49]

* XRD-X-ray diffraction, FTIR-Fourier transform infrared spectroscopy, ATR-IR-Attenuated total reflection-infrared spectroscopy, UV–Vis-Ultraviolet–visible spectrophotometry, AFM-Atomic force microscopy, XPS-X-ray photoelectron spectroscopy, Raman-Raman spectroscopy, FT-Raman-Fourier transform Raman spectroscopy, PL-Photoluminescence spectroscopy, Fluorescence spectroscopy (to analyze fluorescence of a material based on its fluorescent properties), SEM-Scanning electron microscopy, FESEM-Field emission scanning electron microscopy, TEM-Transmission electron microscopy, HRTEM-High resolution transmission electron microscopy, TGA-Thermogravimetric analysis, DSC-Differential scanning calorimetry, HPLC-High-performance liquid chromatography, GCMS-Gas chromatograph mass spectrometry, DLS- Dynamic light scattering, Zeta potential-the potential difference that may exist on the surface of a solid particle immersed in a conducting liquid and the bulk of the liquid, Electrical conductivity-measurement of the current carrying capacity of a given material.

2.2.2. Microstructural studies of GO and RGO

The microstructure and elemental mapping of both GO and RGO were studied by using TEM and HRTEM techniques as well as EDX analysis by using a conventional machine (Tecnai G^2 30, S-Twin, FEI, The Netherlands, 300 kV). The SAED patterns of GO and RGO were also recorded by utilizing the same machine. The EDX analyses were done to estimate the carbon (C) and oxygen (O) contents in GO and RGO.

2.2.3. Raman spectroscopy

Using exposure times of 5–10s and spot size ~5 μm, the Raman spectra of G, D and 2D bands in GO and RGO at 400–3500 cm^{-1} were recorded in a Raman spectrometer (STR500, Technos Instruments, Seki Technotron, Japan) at relatively lower power levels of 532 nm; to avoid the laser heating. To check reproducibility of the results, all measurements were repeated at least five times. Further, many different locations of each examined sample were used to collect at least 10–20 spectra to split up the effect of the substrate from the spatial alterations in the G layer properties and to ensure the reproducibility of the experimental data. Furthermore, the sensitivity of the 2D-band to the number of layers was described by the double resonant model assumed for the G material.

2.2.4. XPS and XRD studies

The C1s core level binding energies of the surface species present in the GO and RGO materials were studied by using the XPS technique (SPECS, Berlin, Germany). The base pressure in the machine was kept at ~10^{-10} mbar. All the measurements were performed using a 12 kV, 200 W X-ray source (non-monochromatic) that utilizes a Mg anode. The hemispherical Phoibos 100 energy analyzer attached in same machine was used to detect the kinetic energy of the emitted electrons. The carbon 1s peak at 285 eV was taken as reference for XPS spectra and these spectra were modelled with combined Gaussian–Lorentzian components including a Shirley background correction. The pass energy of 187.85 eV with step increment of 1.6 eV was used to obtain the survey spectrum and pass energy of 11.75 eV and step increment of 0.1 eV was used to record the individual spectra. The final deconvolution for curve fitting of the experimentally obtained data was done by the XPS CASA software available in the XPS machine itself. The XRD pattern of GO and RGO materials were obtained using a standard diffractometer (X'pert Pro MPD, PANalytical, The Netherlands; 40 kV, 30 mA, $CuK_{\alpha 1}$ radiation; step size 0.05°, residence time at each step – 2 s). The measurements were repeated several times to check the reproducibility of the recorded data.

2.2.5. AFM and GCMS studies

The surface morphology and thickness of the RGO layer was studied by the AFM technique (Veeco Nanoscope IIIa, imaging area ~1 sq. μm, scanner resolution ~0.3 nm) in both contact and tapping modes. The RGO solution drop was put on the silicon oxide substrate. Subsequently, it was dried gently with a blower. Thus, the 3D AFM images gave the lateral dimensions of RGO layers. The tapping mode AFM was used to measure the thickness of few RGO layer stacks on silicon dioxide surface. The standard GCMS technique (GCMS QP 2020EI plus, Shimadzu, Tokyo, Japan) was used to study the different chemical functional groups which constitute the extract of TO. The technique could convert chemical mixture into individual substances when heated and identify the elements at a molecular level. The machine was equipped with an auto-sampler and an auto-injector. The carrier gas used was Helium.

3. Results and discussion

3.1. UV–Vis spectroscopic studies

The UV–Vis absorbance spectra of both GO and RGO samples are shown in Fig. 1. The UV–Vis spectrum of GO shows an absorption peak at 232 nm. This peak is attributed to the π–π* transitions of the aromatic C–C bonds. This spectrum also shows a slight hump at about 300 nm. This hump occurs due to n–π* transitions of C=O bonds present in GO. However, on reduction of GO to RGO, the characteristic absorption band at 232 nm disappears. In fact, this peak is red shifted to about 272 nm in RGO. It happens due to the partial restoration of π network through the revival of electronic conjugation within the RGO sheets [31] obtained after reduction of GO to RGO by the TO extract.

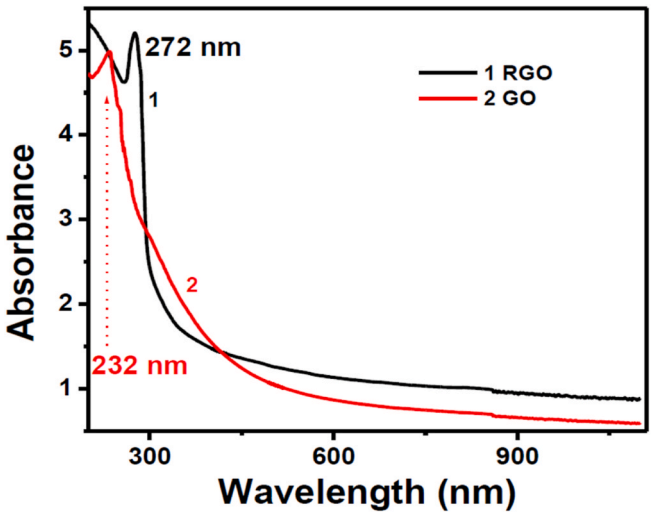

Fig. 1. UV–Vis absorption spectra of GO (1 mg ml^{-1}) and RGO (1 mg ml^{-1}).

3.2. FTIR spectroscopic studies

Fig. 2 (a) and 2 (b) show the FTIR spectra of GO and RGO, respectively. In FTIR spectroscopy generally, GO exhibits absorption bands or characteristics peaks ranging from 900 to 3500 cm^{-1}. Generally, bands that occur at about 1700–1750 cm^{-1} are attributed to carboxyl i.e., (-COOH) groups present mostly at the edges of GO sheet. Similarly, bands present at about 1040–1170 cm^{-1} are attributed to C–O alkoxy stretching vibrations. On the other hand, the bands present in the range of about 3300–3500 cm^{-1} are usually ascribed to O–H stretching vibrations. Further, the bands occurring in the range of about 1300–1400 cm^{-1} are linked to O–H deformations. Furthermore, the bands observed in the range of about 1000–1280 cm^{-1} are associated with stretching vibration of epoxy C–O functional groups. Finally, the bands appearing at the range of about 1600–1650 cm^{-1} are attributed to aromatic C=C stretching vibrations [12,13,31,71].

Fig. 2 (a) shows intense bands at 1217, 1366, 1382, 1632 and 1738 cm^{-1}. Thus, the band at 1217 cm^{-1} happens due to stretching vibration of epoxy C–O functional group [71] or due to C–O–C stretching [31]. Similarly, the bands at 1366 cm^{-1} and 1382 cm^{-1} occurs due to O–H deformation or bending vibration [65,71]. The band at 1632 cm^{-1} occurs due to the stretching vibrations of aromatic C=C functional groups. The band present at 1738 cm^{-1} occurs due to C=O stretching or due to the presence of carboxylic group present most likely at the edges of the GO sheet [31,71]. The slightly blunt band at 1052 cm^{-1} occurs due to stretching vibration of alkoxy C–O functional group [31,71]. The broad hump at 3335 cm^{-1} is due to O–H stretching vibrations [71] suggesting thereby, the presence of functional hydroxyl groups at the surface [31]. These data suggest the presence of various functional groups which contain oxygen [31,71]. Further, the data from present work match with literature data [29,30,32–42,44,45,47]. The reduction of GO to RGO is confirmed from the absence of the band at 1632 cm^{-1} which occurs due to the stretching vibrations of aromatic C=C functional groups (Fig. 2b). The reduction of GO to RGO is confirmed further from the significant reduction in intensity of the broad hump at 3335 cm^{-1} that occurs due to O–H stretching vibrations. Similar observation is reported by other

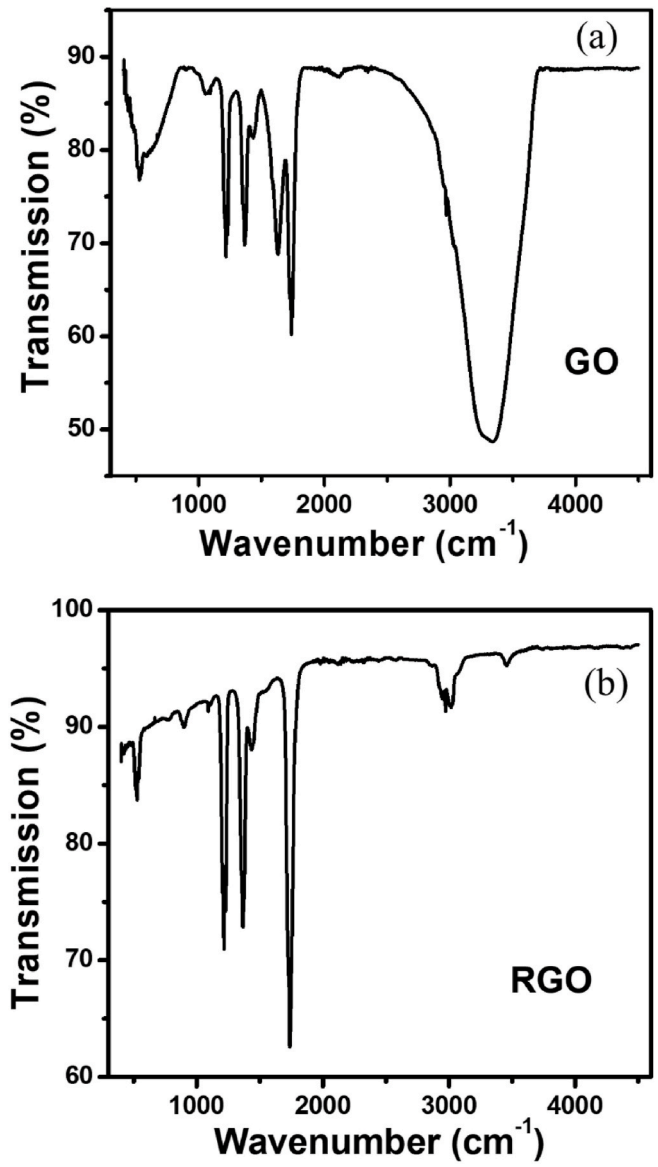

Fig. 2. FTIR spectra of (a) GO and (b) RGO.

researchers using tea polyphenol [37–39] and L ascorbic acid [55] as green reductants to reduce GO to RGO. It may also happen that the alkoxy and epoxy vibration peaks remain almost undistorted in RGO even though their relative positions may slightly change [68]. It is a situation that pertains to partial reduction of GO that is most likely the case of the present work. It needs to be noted further that, when GO is reduced to RGO, it becomes hydrophobic. This process makes the C=C structure partially restored. Consequently, the C=C stretching vibration become dominant but shifted to 1740 cm^{-1} in the RGO (Fig. 2b). Thus, the results obtained from UV–Vis spectroscopy and FTIR spectroscopy (Figs. 1 and 2) techniques corroborate with each other. These results also prove the presence of various functional groups in GO as well as the fact that reduction of GO leads to formation of RGO in the present work. Further, the present results agree with those reported by other researchers [13,29,30,32–42,45,47,55,68,71].

3.3. TEM studies

The HRTEM photomicrograph of microstructure and corresponding SAED pattern of sheet of GO are presented in Fig. 3 (a) and (b), respectively. The GO microstructural sheet shown in Fig. 3 (a) is of 3–5 μm size in width with wrinkle on the edges, as expected due to the intrinsic nature of graphene [13,55,71,88]. From SAED pattern shown in Fig. 3 (b), the bright spot of hexagonal pattern of GO is observed. This is expected because the sheet of GO possesses hexagonal SAED pattern [55,88]. It confirms the short-range crystalline nature of the GO material. The short-range order is over the length scale of the coherence length of the electron beam. The multiple hexagonal rings with different spots reveal the presence of domain boundaries in the selected region. It also confirms the presence of long-range orientational order. The positions of diffraction peak are undifferentiated from those of graphene. Folds or wrinkles in few sheets overlay further rotationally misaligned hexagonal arrangements. This observation also confirms the presence of few layer GO stacks in the microstructure. Similar observations have been reported by other researchers also [13]. Finally, ring patterns are formed most likely due to the increase in the degree of misalignment in the hexagonal arrangements, Fig. 3 (b) [34,49,52].

In a similar way, the TEM photomicrograph of microstructure and corresponding SAED pattern of RGO are shown in Fig. 3 (c) and (d), respectively. The TEM photomicrograph shown in Fig. 3 (c) also confirms the presence of few layer RGO stacks with wrinkles suggesting that both conformal and non-conformal overlap of the few layers RGO stacks and their curling back on themselves happen in the microstructure, as expected [13]. It is evident that the RGO layer is about 2 μm wide. The corresponding SAED pattern of RGO (Fig. 3d) shows the diffused rings. These rings signify a structure that certainly differs from that of GO. It happens because the GO has undergone chemical reduction to RGO. Further, the RGO exhibits bright, focused diffraction spots in the SAED pattern. This happens due to the polycrystalline structure of RGO [13,49,59]. This result confirms the reduction of GO to RGO. Due to the reduction, the inter layer coherence of GO is lost [71]. As a result of this process, more and more oxygen free sheets become randomly oriented [13,49,59,71]. It is this random orientation of these oxygen free GO sheets that gives rise to the polycrystalline SAED ring pattern in RGO (Fig. 3d). Thus, the present results are in tune with what have been reported by other researchers [13,34,49,52,55,59,71,88].

Further, as shown in Fig. 4 (a); the elemental C and O contents in GO are about 78.87% and 8.87%, respectively. Thus, the C/O ratio is about 8.90. Similarly, as shown in Fig. 4 (b); the elemental C and O contents in RGO are about 97.49% and 0.63%, respectively. Thus, the O content is significantly less in RGO, as expected. Hence, the C/O ratio is significantly enhanced to about 154.74. Similar change in C/O ratio are also reported by other researchers albeit the absolute magnitudes are different [34,37–39,51,55,58,67,69–71]. Even, a C/O ratio of as high as 246:1 is reported also in literature [89]. These facts can be rationalized with the view that depending on the method used to reduce GO to RGO, and the intrinsic complexities involved in the chemical structure of the reductant itself; the different C:O ratios are obtained [34,37–39,51,55,58,67,69–71,89]. In the present study, the reduction of GO into RGO is done using extract of TO; as mentioned earlier. The huge reduction in oxygen content is certainly due to the antioxidant characteristic of Alpha Tocopherol [79–85] present in TO seeds extract utilized in the present work.

Further, the Cu peaks in Fig. 4a and (b) occur due to the corresponding Cu coated grids used as GO and RGO sample holders for TEM examinations. There is also a very minor presence of Ca and Mg which might have come as impurities from the graphite resource [90]. But their presence is almost insignificantly small (Fig. 4 a) and should not affect the main results obtained in the current work. On reduction of GO to RGO by TO, a lot of complex chemical reactions have occurred and during this reduction process these impurities might have been either removed or might have been reduced to imperceptibly small magnitude and hence, undetectable in the EDX spectrum shown in Fig. 4 (b).

Moreover, in both Fig. 4 (a) and (b), the relative count of electrons corresponding to the different Cu peaks vary. This is only obvious as the different Cu peaks represent different shells in the electronic configuration of Cu. It is well-known that each element has characteristic peak

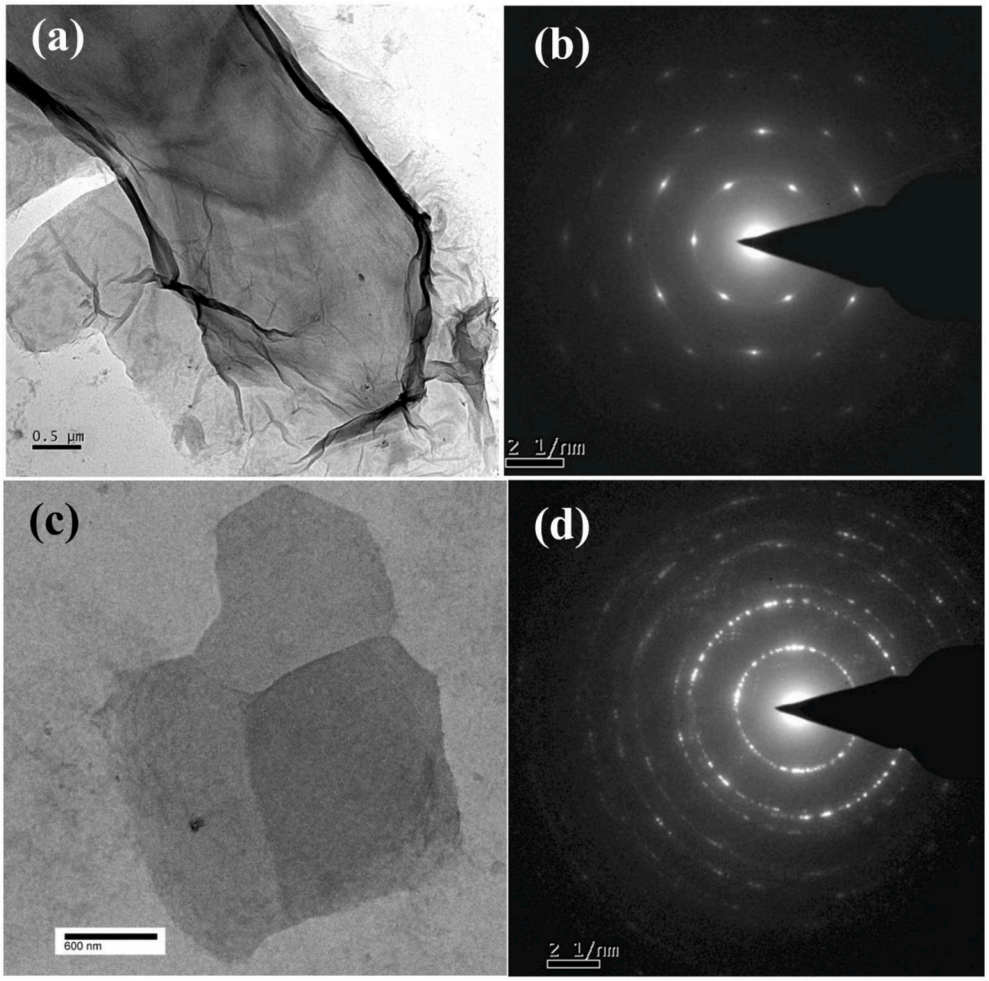

Fig. 3. HRTEM image of (a) GO, (b) SAED of GO, (c) RGO and (d) SAED of RGO.

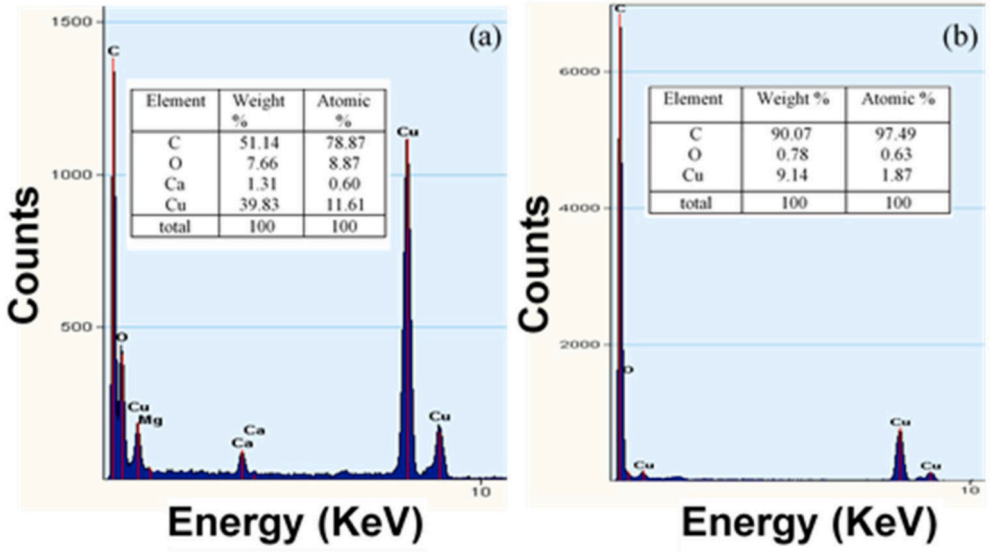

Fig. 4. EDX spectra of (a) GO and (b) RGO.

positions corresponding to the possible transitions in its electron shell. The presence of Cu, for example, is indicated by two K shell corresponding peaks at about 8.0 and 8.9 keV and a L shell corresponding peak at 0.85 eV. Also, there are several almost coincident satellite peaks present due to contributions from the relevant sub-shells which is well established in standard X-ray physics. These may often overlap for many elements making a precise determination of their exact energy positions a real challenge. Hence, this entire data analysis is very high-end

sophisticated software driven in all modern EDX machines attached to TEM as well as FESEM machines. Further, the relative counts vary depending on the instantaneous population distribution function of the electrons in different shells following quantum mechanical restrictions and statistical process physics of characteristic X-ray emission from electron pertaining to a given shell and/or sub-shell and their excitation probabilities. Furthermore, it also depends upon several other factors such as (a) the statistical distribution of energies of the bombarding electrons (b) the recognition mechanisms of the electron emission process itself by the detector and (c) the recording mechanisms of the relevant shell's electrons by the corresponding recording counter in the EDX system. However, these may vary greatly among machines and detectors. It is also very interesting to note that results from TEM studies and EDX analyses are in tune with the results obtained from UV–Vis and FTIR spectroscopic studies which confirm the successful partial reduction of GO to RGO by the TO seeds extract used in the present work.

3.4. Raman spectroscopy studies

Fig. 5 shows the Raman spectra of GO and RGO. The Raman spectra of graphite and G materials consist of mainly three different peaks e.g., two strong peaks D and G and a relatively weaker peak i.e., 2D [91,92]. These peaks lie in the spectral range of 1200–2800 cm^{-1}.

For the present GO material, the D band occurs at 1353 cm^{-1}. The D band occurs due to the structural imperfections. It is suggested by other researchers [71] that the D band could be associated with breathing mode of K point phonons. In particular, the K point phonons belong to the A_{1g} symmetry. The D -band signifies two aspects of GO. The first aspect that the D-band indicates is mainly the disorders that exist in the surface. The second aspect that the D band indicates is the degree of defects in GO [13,34,50–58,71].

Further, the G band occurs at 1585 cm^{-1}. It occurs due to the in-plane vibrations of the sp^2 carbon atoms and a doubly degenerated phonon mode i.e., the E_{2g} symmetry at the Brillouin zone center [93]. In other words [94], it occurs due to the first order scattering of E_{2g} phonon from sp^2 carbon atoms. Thus, the G band indicates the extent of graphitic composition of the GO material.

Similarly, the 2D band of GO occurs at 2690 cm^{-1}. It is observed at nearly double the frequency of D band, as expected for a few layer stacks of GO structure [13]. It originates from the second order Raman scattering process. The changes in shape and intensity of the 2D peak give the information of different states of the G materials. The G peak of RGO is red shifted to 1580 cm^{-1}. Thus, it occurs close to the G peak that occurs at 1563 cm^{-1} [71]. These facts suggest the restoration of the graphitic sp^2 network in the RGO structure [13]. These results again confirm that the GO is reduced to RGO by the extract of TO seeds.

The intensity ratio of D band and G band is often used to check the extent of reduction of GO into RGO [91–99]. Depending on the synthesis process used for reduction of GO to RGO, the ratio I_D/I_G of the intensities of the D band to G band is reported to increase [13,34,48,50–58,60,65,67,69–71,91–96] as well as decrease [97–99]. In the current work the intensity ratio I_D/I_G decreases from 0.58 to 0.14 on reduction of GO to RGO, Fig. 5. Thus, the present observation matches with those reported by other researchers [97–99].

The decrease in ratio of I_D/I_G in RGO represents the higher degree of graphitization, suggesting thereby a decrease in degree of defects [97–99]. It is attributed to the decrease in the sp^2 domain size of carbon atoms and the decrease of sp^3 to sp^2 carbon during the reduction of GO to RGO [97,98]. Thus, it means the restoration of the graphitic sp^2 network in carbon materials [97]. Other researchers [99] also report similar results, as mentioned above. It is ascribed to self-restoration of graphite by slow exclusion of oxygen as well as other functional groups from the partially reduced GO [99]. Thus, from the Raman spectra results obtained in the present work; it is once again confirmed that the partial reduction of GO to RGO is obtained by the extract of TO seeds. Further, these results corroborate well with the results obtained by UV–Vis, FTIR spectroscopic and TEM studies.

3.5. The XPS studies

The typical low-resolution survey spectra of GO and RGO are shown in Fig. 6. It exhibits that the C1s peaks of GO and RGO occur at binding energy (BE) of about 284 eV. Similarly, the O1s peaks of GO and RGO occur at BE of about 530 eV.

Further, the deconvoluted, high resolution XPS spectra of C1s in GO and RGO are shown in Fig. 7 (a) and Fig. 7 (b), respectively. According to other researchers [100], C1s spectrum of GO and RGO comprises of several different elemental peaks connected to possible presence of various surface functional groups. For instance, the peak at BE of about 284.6 eV is associated with the presence of C–C surface functional group [71,100]. Similarly, the peak at BE of about 285.6 eV is associated with the presence of C–OH functional group at the surface. In a similar manner, the peak at BE of about 286.8 eV is attributed to the presence of

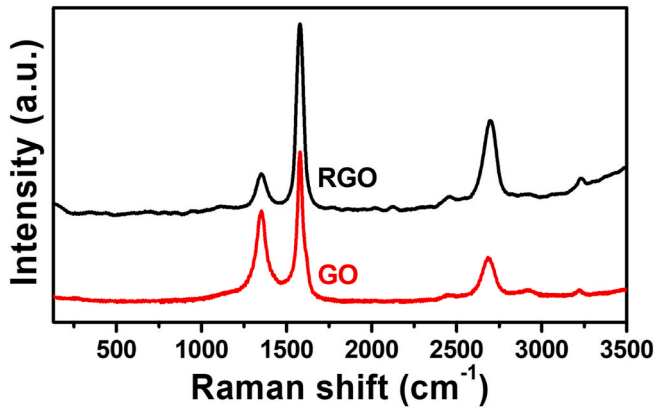

Fig. 5. Raman spectra of GO and RGO.

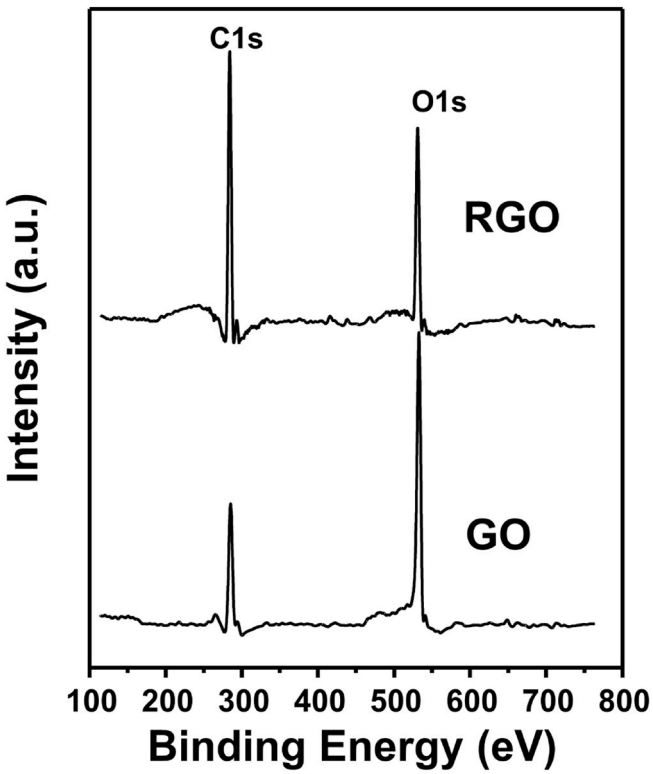

Fig. 6. XPS survey spectra of GO and RGO.

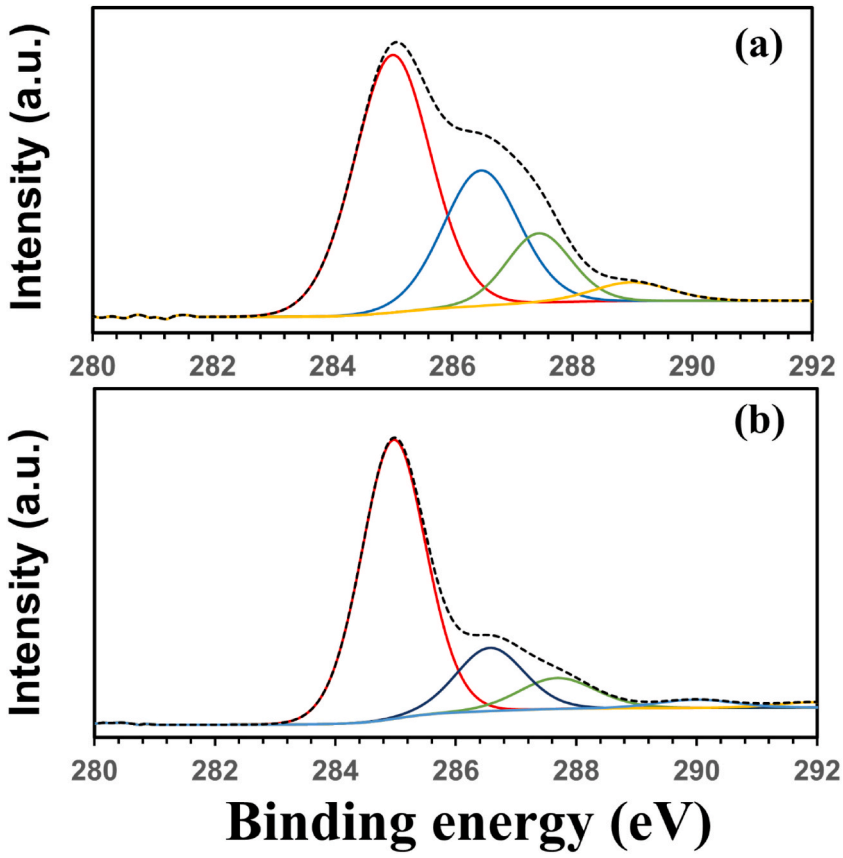

Fig. 7. High-resolution XPS spectra: C1s spectra of (a) GO and (b) RGO.

C-epoxy surface functional group. Further, the presence of a peak at BE of about 288.2 eV BE is associated with the presence of C=O functional group at the surface. Furthermore, the peak at BE of about 289.4 eV is associated with the presence of O–C=O surface functional group [71, 100]. However, it is usually difficult to exactly pinpoint the precise positions and hence, the corresponding BEs of these peaks [100]. Thus, it is evident from the XPS spectrum presented in Fig. 7 (a) that the current GO material bears a relatively larger proportion of oxygen associated with various functional groups present on the surface. Further, relatively minor proportion of oxygen is linked with hydroxyl and –COOH groups on the surface of GO.

On the contrary, the deconvoluted, high resolution XPS spectrum of C1s in RGO represented in Fig. 7 (b) shows that amounts of majority of oxygen-containing functional groups are hugely reduced. The relative intensity of peak at BE of about 284.6 eV (Fig. 7b) corresponding to the C–C functional group is hugely enhanced in RGO. On the other hand, the relative intensity of the peak at BE of about 286.6 eV (Fig. 7b) corresponding to oxygen containing surface functional group of C in C–O is diminished in RGO. Further, the relative intensity of peak at BE of about 287.6 eV (Fig. 7b) corresponding to the presence of carbonyl group at the surface is diminished in RGO. In addition, the relative intensity of peak at BE of about 289.2 eV (Fig. 7a) corresponding to the presence of the functional carboxylate carbon O–C=O group at the surface is diminished in RGO. All these evidences confirm the partial reduction of GO to RGO by the extract of TO seeds, used for the very first time in the current work. In addition, it is fascinating to note that the present results of XPS analysis are in complete agreement to those reported by other researchers [19,20,22,24,55]. The present results also confirm that the extract of TO seeds is successful in restructuring the characteristic graphitic sp^2 network through the reduction of GO to RGO. It is important to note in this context that, the electrical and optical properties of carbon-based materials such as GO and RGO are determined by the π–electrons in the characteristic graphitic sp^2 network [13,71]. Further, these results corroborate well with the results obtained by UV–Vis, FTIR spectroscopic studies as well as those from HRTEM, EDX and Raman spectroscopic studies.

3.6. The XRD studies

The XRD patterns of GO and RGO are shown in Fig. 8. Here, the GO shows the characteristic peak at 2θ value of 11.5°. It corresponds to interlayer spacing of 0.773 nm. It is well-known [38] that the characteristic peak of G occurs at 2θ value of 26.7° with an interlayer spacing of 0.334 nm in the corresponding XRD pattern. The increase in interlayer spacing of GO compared to that of the G sheet occurs due to the presence of oxygen comprising functional groups on the G sheet. These are induced during the oxidation process. The presence of oxygen functional group leads to weak Van der Waals' force interactions between the G sheets. As a result, the sheets exfoliate. This physical process results in the increase of interlayer spacing. Similar explanations are also suggested by several other researchers [13,19–22,29–34].

Here, the RGO shows the characteristic peak at 2θ value of 27.5° corresponding to the (002) plane of the corresponding XRD pattern. It corresponds to interlayer spacing of 0.355 nm. The shift of the GO peak from the 2θ value of 11.5° to the 2θ value of 27.5° in RGO happens on reduction GO to RGO by using the extract of TO seeds. These XRD patterns thus confirm the reduction of GO to RGO. The similar observations of peaks for both GO and RGO are also reported by other researchers in the correspondingly relevant XRD patterns [13,19–22,29–34,40–42,71, 98]. Further, these results (Fig. 8) corroborate well with the results already obtained by the UV–Vis, FTIR spectroscopic, TEM, Raman spectroscopic and XPS studies.

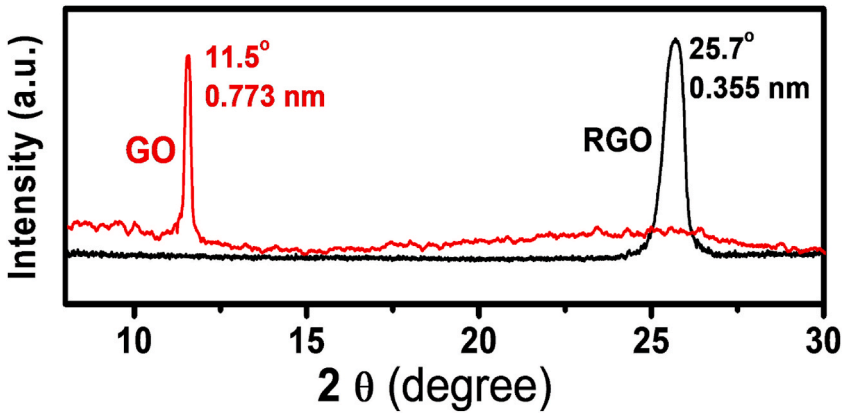

Fig. 8. XRD patterns of GO and RGO.

3.7. The AFM studies

While preparing the sample by drop casting method on to the flat surface of silicon dioxide, more often than not; *the large number of RGO layers were generally observed to be not only overlapped but also curled back on itself, thereby giving relatively higher thickness of about 10 to* 20 nm while measured by AFM. Fig. 9 (a) shows a typical, illustrative example of such a common scenario observed during the AFM measurements.

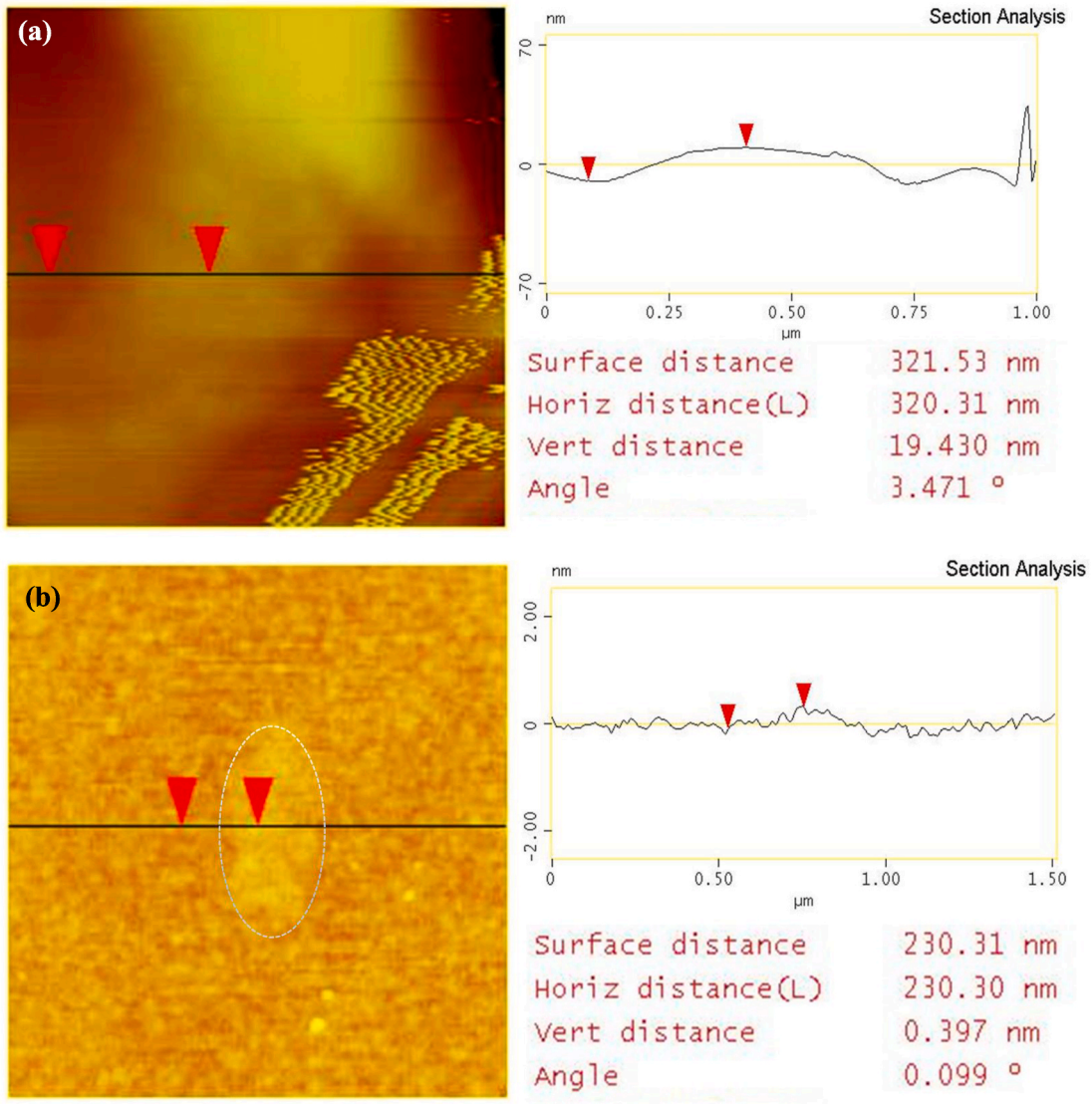

Fig. 9. Tapping-mode AFM images and profile curves of RGO on silicon dioxide (a) few layer stacks of RGO overlapped and self-curled back as a bunch on to themselves and (b) single layer. (For interpretation of the references to color in this figure legend, the reader is referred to the Web version of this article.)

The relatively higher thickness of about 19 nm may be due to several possible reasons: (a) the presence of relatively more stacks of RGO layers, (b) the presence of functional groups attached on both sides of the RGO layers and (c) the most likely process of overlapping on one another followed by self-curling back collectively as a bunch on to themselves. Thus, the actual thickness of such RGO few layer stacks may be about 5–10 nm. It may be recalled here that similar observations are also reported by other researchers [13]. It may be that due to wrinkling followed by the process of self-curling back as a bunch on to themselves, a relatively higher apparent thickness of about 19 nm is found from the AFM measurements, Fig. 9 (a). It is this process of overlapping and self-curling back onto itself, that gives rise to the observation of few layers RGO stacks in the TEM studies of microstructure (Fig. 3 c) in the present work. Thus, the results from the AFM study corroborate well with the results obtained from the TEM studies of the microstructure of RGO.

Eventually, a single layer was also *accidentally* observed *only in a specific position* on the surface of silicon dioxide and hence, must not be considered as a general observation (Fig. 9 b). As a matter of fact, such single layer RGO structures are visible mostly in the case of RGO grown by the CVD process [11]. As such, the presence of single RGO layers is highly unlikely in chemical processes of RGO synthesis [13,29–32]. However, the AFM image and corresponding height profile give the thickness of the single RGO sheet as 0.397 nm. This value *incidentally* matches with the thickness (e.g., 0.335 nm) reported [89] for a monolayer graphene. However, this match should be considered more in a sense of *apparent similarity and absolutely nothing* beyond that. The results of the AFM studies indicate generally the formation of few layers of RGO stacks overlapped on to each other as well as curled back collectively as a bunch on to themselves.

Further, all the results discussed above confirm beyond doubt the excellent, novel capability of the extract of TO seeds for reduction GO to RGO. Therefore, it is of prime importance to understand the compounds present in TO by GCMS as discussed earlier; so that the mechanism responsible for the partial reduction of GO to RGO can be identified. The results of this attempt are presented below.

3.8. The GCMS studies

The chemical compositions of the extract of seeds of TO as evaluated by using GCMS, are shown in Table 2. The corresponding gas chromatograph is shown in Fig. 10. The quantitative estimation of 30 compounds shown in Table 2 is done using the area normalization procedure from the chromatograph data plot presented in Fig. 10. The mechanism responsible for reduction of GO to RGO by the TO material used in the current work for the very first time is discussed below in section 3.9.

The discussion is initiated first based on what is already known from existing literature [29–49] on plant part extract based green reductants thereby, leading to a summary of the state-of-the-art knowledge in this domain. Next, the possible mechanisms responsible for the current results are discussed with this background knowledge in mind.

3.9. Mechanisms responsible for reduction of GO to RGO by TO

It seems plausible to argue that the mechanisms responsible for reduction of GO to RGO needs to be discussed from the perspective of wealth of literature, Table 1 [29–49] that is already presented before but not discussed in detail. It is high time that the same be discussed. The facts given in Table 1 establish a few realities.

The first fact is that fruit extract [29], flower extract [30,31], leaf extract [42,43,45,46], seed extract [35], root extract [33,34], fruit juice [36,44], green tea solution [37–39], rose water [40], coconut water [41], fruit peels [42], spice extract [32], starch [47], tannin extract [48] as well as bark extract [49] are successfully used to reduce GO and RGO. All these plant parts contain a multitude of biochemical compounds with various functional groups [29–49]. This universal success in reduction of GO to RGO generally makes a concern whether some generic mechanisms are active through different biochemical pathways naturally present in correspondingly different plant parts. This issue shall be discussed soon in further details with reference to the wide variety of

Table 2
Chemical composition of TO seeds extract obtained by GCMS study.

Peak	R. Time	Area	Area%	Height	Height%	A/H	Name
1	5.02	160312	2.18	60957	3.9	2.63	
2	5.09	87684	1.19	38075	2.43	2.3	Benzaldehyde
3	5.396	55532	0.75	29787	1.9	1.86	1-Decene
4	5.521	51838	0.7	25797	1.65	2.01	Undecane
5	5.744	34790	0.47	23863	1.53	1.46	3-Carene
6	9.635	333203	4.52	135006	8.63	2.47	1-Tridecene
7	9.874	57900	0.79	25846	1.65	2.24	Dodecane
8	12.413	42571	0.58	13475	0.86	3.16	2-Hydroxy-iso-butyrophenone
9	16.264	388648	5.27	117195	7.49	3.32	1-Tetradecene
10	17.27	77299	1.05	22677	1.45	3.41	Caryophyllene
11	18.556	67831	0.92	21375	1.37	3.17	1,4,7,-Cycloundecatriene, 1,5,9,9-tetrame
12	23.682	277560	3.77	72849	4.66	3.81	1-Heptadecene
13	24.134	375556	5.1	98314	6.29	3.82	Cedrol
14	24.791	37108	0.5	10953	0.7	3.39	Benzophenone
15	30.822	121083	1.64	32852	2.1	3.69	1-Heptadecene
16	32.269	49654	0.67	14217	0.91	3.49	Neophytadiene
17	37.42	69119	0.94	19275	1.23	3.59	Trifluoroacetic acid, pentadecyl ester
18	37.735	44687	0.61	11953	0.76	3.74	Naphthalene, decahydro-1,1,4a-trimethyl-
19	42.834	106013	1.44	26550	1.7	3.99	(1R,4aR,4bS,7R,10aR)-1,4a,7-Trimethyl-
20	42.957	73935	1	19666	1.26	3.76	1,3,6,10-Cyclotetradecatetraene, 3,7,11-tr
21	43.746	215581	2.93	55383	3.54	3.89	1,3,6,10-Cyclotetradecatetraene, 3,7,11-tr
22	44.301	93790	1.27	24061	1.54	3.9	(E)-3-Methyl-5-((1R,4aR,8aR)-5,5,8a-tri
23	46.33	198080	2.69	44631	2.84	4.44	2-Phenanthrenol, 4 b,5,6,7,8,8a,9,10-octah
24	46.813	118654	1.61	28731	1.84	4.13	Ferruginol
25	50.104	132373	1.8	32737	2.09	4.04	1-Naphthalenepropanol,.alpha.-ethenylde
26	54.97	701136	9.51	96059	6.14	7.3	
27	55.01	463450	6.29	91266	5.83	5.08	
28	58.759	1870803	25.39	299768	19.17	6.24	1-Naphthalenepentanoic acid, decahydro-
29	60.022	828497	11.24	52327	3.35	15.83	
30	61.430	234101	3.18	18488	1.18	12.66	Alpha Tocopherol

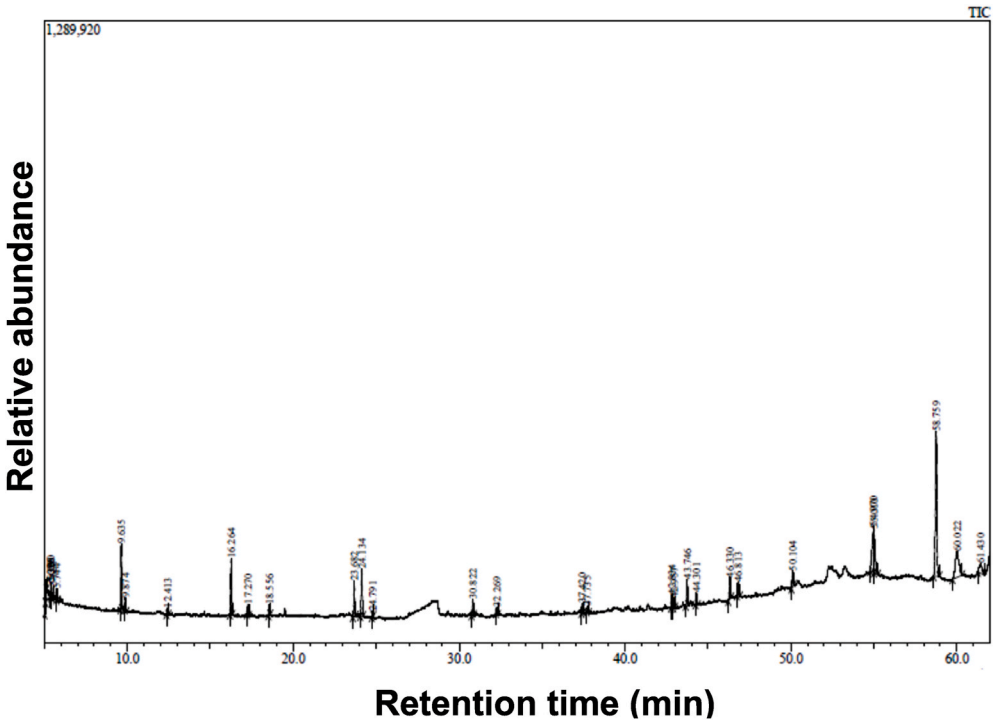

Fig. 10. GCMS chromatogram of the extract of TO seeds.

mechanisms suggested by a multitude of researchers [29–49]. Further, the reduction of GO to RGO can happen at room temperature (RT) [34,42,49]. However, several reports also involve use of various temperature ranges, Table 1 [29–33,36–41,43–48]. The usage of relatively higher temperatures may be rationalized in terms of enhancing the reaction kinetics of the reduction process of GO to RGO.

Despite the wealth of literature, however, each step of the relevant biochemical process and/or processes of the reduction of GO to RGO has remained far from well-defined so far. This is possibly also the reason that the journey continues with ever growing vigor and focus [13,29–32].

The second fact is that although utilizing different parts of the plants and hence, different specific sources of biochemical pathways, the most common experimental characterization techniques used [29–49] to prove the reduction of GO to RGO are e.g., UV–Vis, FTIR, XPS, TEM, HRTEM, EDX, Raman, XRD and AFM. *Similar techniques are utilized in the present work*. Further, some additional techniques like thermo-gravimetric analysis (TGA), scanning electron microscopy (SEM) and electrical conductivity are occasionally utilized [44]. Furthermore, fluorescence and high-performance liquid chromatography (HPLC) techniques have been rarely used [44]. In only one occasion, GCMS has been utilized [45]. *It is interesting to note that the present study also utilizes the GCMS technique* (Table 2, Fig. 10).

The third fact is that many compounds are often suggested to be responsible for the reduction of GO to RGO. *There is in fact nothing wrong with it as this is possibly closest to the exact truth, to dig out which; each step of the corresponding highly complex biochemical reaction and the corresponding kinetics of the biochemical reaction process and/or processes; are needed to be elucidated. But since multiple chemical compounds are involved; this is difficult to be experimentally followed up in exact details.*

For instance, it has been suggested [29] that reduction of GO to RGO by emblica officinalis fruits happens due to the presence of several compounds e.g., vitamin C, pectin, flavonoids, alkaloids, terpenoids, quercetin tannins, gallic acid, phyllaemblic compounds, and polyphenolic compounds. *It is an absolute reality that the relative contributions of each of these compounds in GO to RGO reduction would be very difficult, if not impossible, to experimentally assess and thereby propose an exact mechanism based totally on this reaction pathway*. That is why the researchers have rightly suggested [29] that the compounds mentioned above are jointly responsible for the reduction of GO to RGO. Following a similar inductive logic, it has been suggested that for the green reduction of GO to RGO, the phytochemicals and antioxidants [30] or only the phytochemicals [31] present in Marigold flower extract are responsible. The logical extension of this philosophy suggests the presence of antioxidants present in clove [32] to be responsible for GO to RGO reduction.

The brief survey of literature (Table 1) therefore presents the further, righteous extension of this philosophy. For instance, it has been suggested that when beta carotene reduces GO to RGO it is possible that the O^{2-} reacts with the epoxide moiety of GO to generate R–CHO and removal of one H_2O molecule [33]. The details of exact reaction mechanisms are not reported [33]. On the other hand, the endophytic microorganisms present in green carrot route are believed to be responsible for reduction of GO comprising of e.g. diol, hydroxyl, epoxide, ketone etc. functional groups to RGO; but the reaction mechanism details are not reported [34]. In a similar philosophy, the antioxidant actions of phenolic parts of curcumin molecule [35] and polyphenols in grape juice [36] are suggested to be responsible for reduction of GO to RGO. However, the details are again not reported [35,36].

On the other hand, the tea polyphenols (TPs) such as about 50–80 wt % EGCG (epigallocatechin gallate) and other polyphenols such as EGC (epigallocatechin), epicatechin gallate (ECG) and EC (epicatechin) are suggested to be responsible for the reduction of GO to RGO with [39] or without the presence of Fe [37,38]. However, due to the complex structure of TPs the exact details of reaction mechanisms are yet to be

well understood [37]. In a similar manner, it has been suggested that the antioxidant activities of phenolic compounds plus flavonol glycosides are responsible for reduction of GO to RGO by rose-water but, the details of reaction mechanism are not reported yet [40]. Thus, several researchers [29,35–40] identify *polyphenols and/or phenolic compounds* as an important component for reduction of GO to RGO although, the exact details of relevant reduction mechanisms are not reported.

A similar situation pertains when the reductant role of C. nucifera (cocos nucifera L) is suggested to be responsible for reduction of GO to RGO by coconut water [41]. In the case where GO is reduced to RGO by other green resources such as citrus sinensis peel, leaves of C. esculenta and M. ferrea linn [42], it is suggested that possibly the reduction of phytochemicals to quinones in presence of ROS leads to reduction of oxygen containing functional groups in GO even though details of reduction mechanism are not reported. In a similar way, the antioxidant properties of glucuronic acid derivatives of flavonoids and tartarated derivatives of p-coumaric acid [43] are suggested as responsible for reduction of GO to RGO by spinach leaves. Thus, it is not surprising to note that a host of compounds e.g., carbohydrates, glycosides, flavonoids, phytosterols, protein etc.; are suggested to be responsible for the reduction of GO to RGO by pomegranate juice although the exact details are yet to emerge [44]. Therefore, it is evident that several researchers suggest *flavonoids* [29,44] *or acid derivatives of flavonoids* [43] are linked to green reduction of GO to RGO.

In a similar extension of this inductive logic it has been suggested that various compounds such as eucalyptols, aldehydes, terpineols, alcohols, amides and ethers of eucalyptus present in eucalyptus leaf extract and experimentally found out by the GCMS characterization technique [45]; are responsible for the reduction of GO to RGO. Thus, several researchers link presence of various terpineol compounds [29,45] to the reduction process of GO to RGO even though the details of reduction mechanism are yet to be amply established. Another recent work [46] suggests the combined presence of many compounds e.g., fatty acids, carotenoids, polyphenols, histamines, phenolic acids and serotonins etc. present in the extract of urtica dioica leaves as responsible for GO to RGO reduction even though the exact details of the relevant mechanisms are yet to be reported. Thus, several researchers [29,35–40,46] identify *polyphenols and/or phenolic compounds* as an important component for reduction of GO to RGO although, the exact details of relevant reduction mechanisms are not reported.

On the other hand, aldehydes and ketones formed under alkaline condition by interaction of GO with OH functional group of starch is thought to be the responsible for reduction of GO to RGO by starch solution [47]. Here also, the details of reduction mechanisms remain yet to be comprehensively reported. When tannin is used, the abundant presence of catechol and pyrogallol is suggested to be responsible for the reduction of GO to RGO [48] although details of the reaction mechanism are not reported. Finally, the antioxidant and free radical scavenging activities of cinnamon-aldehyde, eugenol and their derivatives present in cinnamon bark is suggested to be the agents [49] for reduction of GO to RGO by cinnamon bark extract. Thus, several researchers [45,47,49] link the presence of *aldehydes* to the reduction of GO to RGO.

To summarize, the brief survey of literature [29–49] prove beyond doubt; that the mechanisms for reduction of GO to RGO by extracts obtained from various plant components are *phenomenologically suggested to be linked to rightful contributions from a multitude of compounds present in the relevant parts but the details are yet to be unequivocally established.* Truly speaking this is *the current state of the art knowledge* and it is certainly growing in right direction [29]. This lack of fundamental knowledgebase is also the major cause of continued current thrust in research on green reductants for synthesis of RGO from GO [13,30–32]. It is therefore imperative that, the present results be also viewed from a similar perspective as well.

The present work uses the extract of TO seeds. As such, TO is an evergreen tree of Cupressaceae Group [72]. The extract of TO seeds contains Tocopherol, alkaloids and fixed oils [72–85]. The extract of TO seeds possesses many good attributes e.g., antioxidant, anticancer and anti-inflammatory properties [72–81]. The antioxidant capacity of TO seeds is linked to the presence of Alpha Tocopherol. It is also commonly known as vitamin E [79–85]. It is also useful for synthesis of NPs [86,87]. The importance of TO extract and Alpha Tocopherol is amply identified in Table 3. Before going into details of vitamin E and Alpha Tocopherol it is advisable to have a basic idea about the processes based

Table 3
Uniqueness of TO and Alpha Tocopherol.

Sample/Issue	Application	Remarks	Ref. No
TO extract	TO extract works as an anthelminthic agent for the treatment of parasitic worms	It destroys the ROS* of parasitic cell and their cell membranes by its antioxidant activities	[73]
TO extract	TO extracts used for anti- uterine cancer treatment	The biotechnological properties, antioxidant properties of TO is useful in these treatments	[74]
TO extract	TO extracts utilized for neurological disorder treatments	The biotechnological properties, antioxidant properties of TO is useful in these treatments	[75]
TO extract	TO extract used for cystitis treatment, rheumatism treatment, amenorrhea treatment, psoriasis treatment, enuresis treatment and bronchial catarrh treatment	The biotechnological properties, antioxidant properties of TO is useful in these treatments	[76]
Extract of TO twigs	Ethanolic fraction of TO twigs extract exhibits significant anti-atherosclerotic property	The antioxidants present in TO reduces ROS* in cells and reduces total as well as LDL** cholesterol levels	[77]
Extract of TO twigs	Ethanolic fraction of TO twigs extract exhibits significant anti-diabetic activities	Glutathione reductase present in TO reduces hydro per oxidase in the presence of Glutathione per oxidase	[78]
Role of Serum Alpha Tocopherol in human mortality risk reduction	Higher intake of serum Alpha Tocopherol causes lower mortality risks	Peroxyl scavenging antioxidant role of Alpha Tocopherol reduces cardiovascular disease mortality risk by 47%	[79]
Role of Alpha Tocopherol in human lipoprotein	Alpha Tocopherol reduces Cu (II) to Cu (I) in human lipoprotein	Cu (II) reduction by the lipoproteins is linked to their alpha tocopherol content	[81]
Role of Alpha Tocopherol in foods and oils	Alpha Tocopherol reduces edible fats and oils	Hydrogen donation by Alpha Tocopherol scavenge free radicals in foods e.g., edible oils and fats	[82]
Role of Alpha Tocopherol in higher plant cells	Alpha Tocopherol protects poly unsaturated fatty acids from oxidation	Alpha Tocopherols do both scavenging and quenching of various ROS as well as the lipid oxidation products	[84]
Ag NPs synthesis by TO leaf extract	Ag NPs synthesis and characterization	Alpha Tocopherol does both reduction of $AgNO_3$ solution and capping stabilization of synthesized Ag NPs	[86]
TO leaf extract mediated Ag NPs synthesis	Cytotoxic and mutagenic attributes in peripheral human blood lymphocytes	Results confirm that for human peripheral blood lymphocytes, the TO leaf mediated Ag NPs have both cytotoxic and mutagenic attributes.	[87]

*ROS-Reactive oxygen species, **LDL-Low density lipoprotein.

on which the plant-based antioxidants generally function.

All plants produce antioxidants [83]. There are many examples of non-enzymatic antioxidants. These mainly include e.g., vitamin C, vitamin E and plant polyphenol. Further, glutathione and carotenoids are also non-enzymatic antioxidants. *Thus, all the aforesaid plant part extracts utilized earlier* [29–49] *exploit basically one or the other of these compounds* [83] *and/or their suitable combinations.* It is thus pertinent to know how vitamin E functions as an antioxidant. Basically, this function is achieved as it interrupts and terminates free radical chain reactions. Vitamin E is soluble in lipids. Other similar antioxidants e.g., carotenoids are also soluble in lipid. All these non-enzymatic lipid soluble antioxidants including vitamin E are in the membranes of the relevant plant cells [83] and hence, are easily available for reduction of GO to RGO [29–49]. It needs to be noted further that vitamin E, vitamin C, carotenoids and glutathione are of small molecular size. They all function in a generic mechanism.

At first, they neutralize the ROS by radical scavenging. Next, they carry them away [83]. As functional oxygen containing groups are also present in GO (e.g., hydroxyl, alkoxyl, epoxide etc.) developed in the present work as well as in literature [29–49], the same generic antioxidant mechanism of Alpha Tocopherol present in vitamin E is, in principle, valid in the case of the present work.

As such, Vitamin E is a family of eight molecules [85]. Each of these molecules, comprises of a chromanol ring. Each chromanol ring possesses an aliphatic side chain. If the side chains are saturated, the group comprises of Tocopherols. Depending on at which of the positions 5, 7 and 8 of the chromanol ring, the specific methyl group is substituted; four isoforms e.g., alpha, beta, gamma, and delta of Tocopherol are formed. It is reported [85] that generally three chiral centers are present in Tocopherols. In addition, three configurations (e.g., 2R, 4′R and 8′R) are most common for Alpha Tocopherol. Further, it is reported [85] that out of the naturally occurring scavengers of ROS, Alpha Tocopherols; which are basically mono-phenolic compounds formed as derivatives of chomanols [82]; provide the highest potential of applications. Due to this intrinsic characteristic they act as excellent antioxidants in foods [82], as a chain breaker in lipid peroxidation [83], as antioxidant in higher plant cells [84], and in therapeutics for prevention of critical disease such as Alzheimer's disease, cardiovascular failure, breast cancer and many other disease [79,85]. Further, due to the same generic intrinsic characteristic it reduces Cu (II) to Cu (I) in human lipoproteins also [81]. Moreover, it has potential roles as both reducing agent and capping agent for synthesis of Ag NPs [86,87]. Thus, its role in synthesis of metal NPs, role in biotechnology and role in antioxidant activities are amply proven already [79,81–87].

During reduction, it terminates the lipid peroxidation chain reaction and; in the process gets oxidized to Alpha Tocopheroxyl radical [83]. The stability of Alpha Tocopherol as an antioxidant comes from the process of resonance delocalization. This delocalization occurs throughout the phenolic ring of Alpha Tocopherol structure [82]. Therefore, this radical is not only sufficiently stable but also sufficiently non-reactive to initiate lipid peroxidation on its own. These are the qualities that makes Alpha Tocopherol present in vitamin E; a good, generic antioxidant material [80,83]. The similar mechanism is applicable to the reduction of GO to RGO in the present work.

Here, the possible mechanisms responsible for reduction of GO to RGO by TO are described in Figs. 10–12. Both from the GCMS data plot (Fig. 10) and from the relative distribution of various chemical compounds present in TO (Table 2), the experimental data also indentify the significant presence of Alpha Tocopherol, the most useful natural antioxidant (Table 3). Thus, Alpha Tocopherol consumes 61.1% of area (A), 1.18% of height (H) and possesses the second highest (A/H) ratio of 12.66 (Table 2) amongst these 30 compounds (given that the area is 184101 units and the corresponding time is 18488 units). Therefore, based on several literature evidence [79–85] and the experimental data generated in the current work (Fig. 10 and Table 2) it seems plausible to argue that Alpha Tocopherol *present in the extract of TO seeds; is responsible for the reduction of GO to RGO*.

Fig. 11 shows a collection of several digital images. The first one is of the original TO. The second one is that of the greenish TO seeds extract used in the present work. The third one represents the synthesized slightly yellow brownish solution of GO. Finally, the fourth one represents *especially*, the rather blackish solution of RGO produced by using this TO seeds extract. The color change of GO suspension on reaction with extract of TO seeds for 6 h, is clearly distinguishable from the third and fourth digital images presented in Fig. 11. From these two digital images it is confirmed that on reduction, the yellow brown color of GO changes to completely black homogeneous suspension of RGO.

The mechanisms of reduction of GO to RGO by TO seeds extract is schematically shown in Fig. 12. In this context it needs to be noted that the lower is the bond dissociation energy (E_{BD}) for O–H group of the monophenolic antioxidants i.e., Alpha Tocopherol present in TO seeds extract, the higher is the stability of the antioxidant [82]. As such, (E_{BD}) for the O–H functional group is ~70–100 KCal.mol^{-1} for the monophenolic antioxidants. Further, it is interesting to note that in terms of magnitude (E_{BD}) Delta Tocopherol > (E_{BD}) Gamma Tocopherol > (E_{BD}) Beta Tocopherol > (E_{BD}) Alpha Tocopherol [82]. This fact confirms further that Alpha Tocopherol possesses the least magnitude of bond dissociation energy of the O–H functional group and hence, it should be rather easy for bond dissociation to happen in it.

In addition, Tocopherol has a small reduction potential of about only 500 mV [101]. On the other hand, hydroxy radical has a reduction potential of 2300 mV [102]. However, alkyl radicals possess a much smaller reduction potential of about 600 mV. Further, the reduction potential is about 1600 mV for the alkoxy radicals. Furthermore, a still

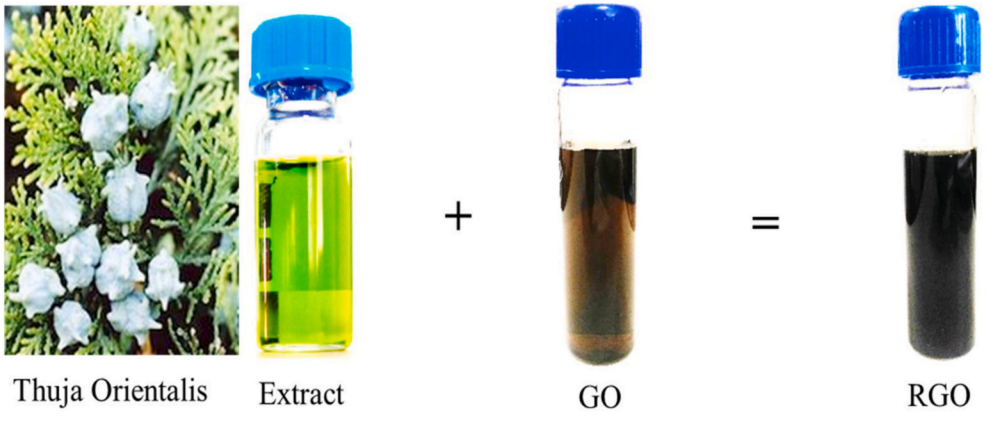

Fig. 11. Digital pictures of TO, extract of TO seeds, GO and RGO.

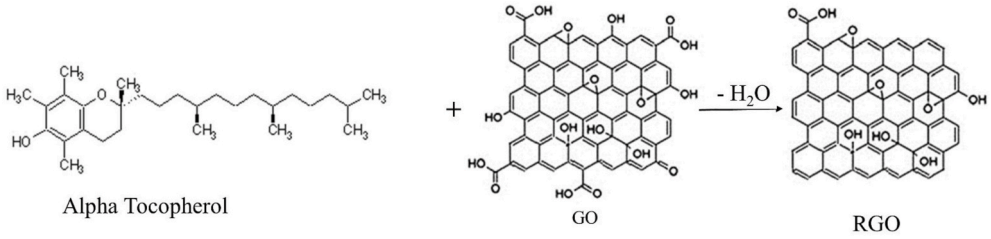

Fig. 12. Proposed reaction mechanisms for the chemical reduction of GO to RGO by Alpha Tocopherol present in the extract of TO seeds.

smaller reduction potential of about 1000 mV is possessed by the alkyl peroxy radicals. On the other hand, superoxide radicals have a reduction potential of about 940 mV [102]. *Thus, the reduction potential of Tocopherol is smaller than those of all the radicals mentioned above. Therefore, it seems plausible to argue that Tocopherol, especially Alpha Tocopherol can easily donate hydrogen to the hydroxy, peroxy, alkyl and alkyl peroxy radicals which may be present in GO and thereby*; *reduce them* [102].

It is indeed reported [82] that *Tocopherol* can donate hydrogen at the 6-hydroxy group. This group is present on a chromanol ring. The donation of hydrogen results in formation of an alkyl hydroperoxide functional group while the *Tocopherol* is oxidized to a stable Tocopheroxyl radical [82], as mentioned earlier. A similar situation pertains in the current work. It is therefore suggested that the reduction of GO to RGO can be thought of as a suitable combination of several chemical reactions [72,103] which happen due to the presence of reactive, oxygen containing functional groups in the surface of GO [29–49] and the monophenolic structure of Alpha Tocopherol [82] that acts as a green reductant in the current work.

As shown in Fig. 12, the compound Alpha Tocopherol possesses a hydroxyl group. Therefore, it can donate a hydrogen atom to reduce the free radicals of GO, as mentioned above. Now, Alpha Tocopherol, the water-soluble antioxidant reacts with the oxidant (GO). Therefore, based on literature evidences [79–85] it is suggested that this reduction process may possibly form the first oxidative intermediate Dihydroxybenzoyl trihydroxy benzofuranone (DTB).

This process donates hydrogen out (Fig. 12). This hydrogen possesses high binding affinity to hydroxyl and epoxide groups. As a result, water is formed. On the other hand, it is suggested already by other researchers that the DTB is irreversibly oxidized to Quinone [104–106]. These products then form the hydrogen bonds with residual oxygen functional group e.g., the peripheral carboxylic groups present in GO (Fig. 12).

Based on all experimental evidences it is therefore suggested that through this reaction pathway perhaps the partial reduction of GO to RGO happen by the action of Alpha Tocopherol present in TO seeds extract. Further, the alkaline pH condition provides the electrostatic steric hindrance between the RGO sheets. This process therefore obstructs the occurrence of the electronic π-π stacking conjugation among the RGO sheets. As a result, the usual process of aggregation is *only partially but not totally* prevented. The culmination of all these process steps finally result in the formation of a stable RGO suspension (Fig. 12).

Further support to the contention that Alpha Tocopherol in TO seeds extract does both reduction and stabilization, comes from several other independent reports [107,108]. For instance, zerovalent iron NPs are synthesized from ferric ions using TO leaf extract [107]. The phenols and reducing sugars present in the extract are suggested to be responsible for the reduction of ferric ions to zero valent iron. These zero valent NPs possess antimicrobial properties as well as anti-bio-film formative properties [107]. Similarly, SiO_2 NPs are synthesized from TEOS (Tetra ethyl ortho silicate) utilizing the TO extract [108]. Presence of phenols in the TO extract is suggested to be responsible for stabilization of the SiO_2 NPs. Further, these NPs have anti-microbial properties [108]. Finally, it is noted that radical scavenging of the oxygen containing functional groups by Alpha Tocopherol present in vitamin E promotes formation of structural defects on the surface of CNT [109]. Thus, summing up [79–85,88–106] it may be suggested that antioxidant properties of Alpha Tocopherol present in TO seeds extract is responsible for the reduction of GO to RGO in the present work.

3.10. The implications

There is a major implication present in the results of the current work. This is the philosophy of synergy between the biofriendly characteristics of RGO [26–32] and the biofriendly characteristics of TO extracts, Table 3 [73–78]. In other words, the reduction of GO to RGO by the green bio-resource e.g., the TO seeds extract should further enhance; at least in principle; the bio-applicability of RGO developed in the present work.

The RGO obtained is also highly dispersible in water and hence, should be amenable to large scale processing. Further, the extract of TO seeds is environmentally benign as well as sustainable. Thus, it provides a greener, new solution to the challenge of using the conventional toxic chemicals for synthesis of RGO. Since, the TO plant is abundantly available in nature; the process parameters can be suitably optimized for large scale green synthesis of RGO.

Going ahead further, such RGO may find important usage in electronic [1], biomedical [2,26–29], anti-microbial [3,30,31], nanomedicine [9], supercapacitors [12,18,33], fast response humidity sensing [19], hydrogen storage [21], PEM fuel cell [22], anodes of lithium ion batteries [23–25], photocatalysis [32], anti-cancer [35], and water treatment [36] etc. applications. If this dream comes true, the TO extract utilized in the current work should find applications not only for GO to RGO reduction but also for aforesaid and many other advanced technological applications [107–109].

4. Conclusions

The reduction of GO to RGO is obtained by using a green reductant, i.e., the TO seeds extract in the current work. To the best of our knowledge, despite the wealth of literature; *the application of TO for this purpose is pioneering in nature*. The reduction of GO to RGO by TO seeds extract is confirmed from results of UV–Vis, FTIR, TEM, HRTEM, EDX, Raman, XPS, XRD and AFM studies. Additional results obtained by the GCMS technique confirm that Alpha Tocopherol present in TO seeds extract is most likely responsible for the reduction of GO to RGO. Based on ample literature evidence as well as the experimental data obtained in the current work; the characteristic, generic antioxidant mechanisms by which; Alpha Tocopherol present in TO seeds extract reduces GO to RGO, are also suggested. In the purview of largescale green synthesis of RGO using the bio-resource of TO extract and its many possible technological fallouts, the implications of the current results are also comprehensively discussed.

Declaration of competing interest

The authors declare that they have no known competing financial interests or personal relationships that could have appeared to influence the work reported in this paper.

Acknowledgements

This work was financially supported by Manipal University Jaipur (MUJ), Rajasthan, India through enhanced seed grant endowment fund project EF/2019-20//QE04-06. The authors thank the Central Analytical Research Facility at MUJ and the Central Research Facility at MNIT Jaipur for GCMS and UV–Vis as well as FTIR characterizations, respectively. The authors also thank IIT Delhi for HRTEM and AFM characterizations.

References

[1] M.K. Rabchinskii, S.A. Ryzhkov, D.A. Kirilenko, N.V. Ulin, M.V. Baidakova, V. V. Shnitov, S.I. Pavlov, R.G. Chumakov, D. Yu Stolyarova, N.A. Besedina, A. V. Shvidchenko, D.V. Potorochin, F. Roth, D.A. Smirnov, M.V. Gudkov, M. Brzhezinskaya, O.I. Lebedev, V.P. Melnikov, P.N. Brunkov, From graphene oxide towards aminated graphene: facile synthesis, its structure and electronic properties, Sci. Rep. 10 (2020) 6902.

[2] O. Yi, G. Choe, J. Park, J.Y. Lee, Graphene oxide-incorporated hydrogels for biomedical applications, Polym. J. (2020), https://doi.org/10.1038/s41428-020-0350-9.

[3] S. Joshi, R. Siddiqui, P. Sharma, R. Kumar, G. Verma, A. Saini, Green synthesis of peptide functionalized reduced graphene oxide (rGO) nano bioconjugate with enhanced antibacterial activity, Sci. Rep. 10 (2020) 9441.

[4] K.S. Novoselov, A.K. Geim, S.V. Morozov, D. Jiang, Y. Zhang, S.V. Dubonos, I. V. Grigorieva, A.A. Firsov, Electric field effect in atomically thin carbon films, Science 306 (2004) 666–669.

[5] C. Cheng, S. Li, A. Thomas, N.A. Kotov, R. Haag, Functional graphene nanomaterials based architectures: biointeractions, fabrications, and emerging biological applications, Chem. Rev. 117 (2017) 1826–1914.

[6] A.K. Geim, K.S. Novoselov, The rise of graphene, Nat. Mater. 6 (2007) 183–191.

[7] Y. Zhu, S. Murali, W. Cai, X. Li, J.W. Suk, J.R. Potts, R.S. Ruoff, Graphene and graphene oxide: synthesis, properties, and applications, Adv. Mater. 22 (2010) 3906–3924.

[8] Pushpendra Kumar, Functionalized Nano-Porous Silicon Surfaces for Energy Storage Application, Springer, Cham, March 2020, pp. 377–393, https://doi.org/10.1007/978-3-030-33774-2_16. In book: nanotechnology for energy and environmental engineering.

[9] H.Y. Mao, S. Laurent, W. Chen, O. Akhavan, M. Imani, A.A. Ashkarran, M. Mahmoudi, Graphene: promises, facts, opportunities, and challenges in nanomedicine, Chem. Rev. 113 (2013) 3407–3424.

[10] K.S. Novoselov, A.K. Geim, S.V. Morozov, D. Jiang, Y. Zhang, S.V. Dubonos, I. V. Grigorieva, A.A. Firsov, Electric field effect in atomically thin carbon films, Science 306 (2004) 666–669.

[11] T. Ohta, A. Bostwick, T. Seyller, K. Horn, E. Rotenberg, Controlling the electronic structure of bilayer graphene, Science 31 (2006) 951–954.

[12] S. Venkateshalu, D. Rangappa, A.N. Grace, Hydrothermal Synthesis and electrochemical properties of CoS_2–reduced graphene oxide nanocomposite for supercapacitor application, Int. J. Nanosci. 16 (2017), 1760020.

[13] D. Rangappa, J. Hoon, J. Honma, Supercritical Fluid Processing of Graphene and Graphene Oxide, in: In book: Graphene - synthesis, characterization, properties and applications, Chapter 4, Source: In Tech Open, September 2011, pp. 45–58. DOI: 10.5772/21783.

[14] K. Chen, D. Xue, S. Komarneni, Nanoclay assisted electrochemical exfoliation of pencil core to high conductive graphene thin-film electrode, J. Colloid Interface Sci. 487 (2017) 156–161.

[15] W.S. Hummers, R.E. Offeman, Preparation of graphite oxide, J. Am. Chem. Soc. 80 (1958) 1339.

[16] T. Szabo, O. Berkesi, P. Forgo, K. Josepovits, Y. Sanakis, D. Petridis, Evolution of surface functional groups in a series of progressively oxidized graphite oxides, Chem. Mater. 18 (2006) 2740–2749.

[17] D. Li, M.B. Muller, S. Gilje, R.B. Kaner, G.G. Wallace, Processable aqueous dispersions of graphene nanosheets, Nat. Nanotechol. 3 (2008) 101–105.

[18] K. Pal, V. Panwar, S. Bag, J. Manuel, J.-H. Ahn, J.K. Kim, Graphene oxide/polyaniline/polypyrrole nanocomposite for a supercapacitor electrode, RSC Adv. 5 (2015) 3005–3010.

[19] K. Rathi, K. Pal, Impact of doping on GO: fast response−recovery humidity sensor, ACS Omega 2 (2017) 842–851.

[20] V. Panwar, A. Chattree, K. Pal, A new facile route for synthesizing of graphene oxide using mixture of sulphuric-nitric-phosphoric acids as intercalating agent, Physica E 73 (2015) 235–241.

[21] M. Kaur, K. Pal, An investigation for hydrogen storage capability of zirconia-reduced graphene oxide nanocomposite, Int. J. Hydrogen Energy 41 (2016) 21861–21869.

[22] T. Roy, S.K. Wanchoo, K. Pal, Novel sulfonated poly (ether ketone)/rGONR@ TiO2 nanohybrid membrane for proton exchange membrane fuel cells, Solid State Ionics 349 (2020), 115296.

[23] M. Shetty, M. Murthy, M. Shastri, M. Sindhusree, H.P. Nagaswarupa, P. D. Shivaramu, D. Rangappa, Hydrothermally synthesized Bi2MoO6/Reduced Graphene Oxide composite as anodes for lithium-ion batteries; Advanced ceramics and nanomaterials for sustainable development, Ceram. Int. 45 (2019) 24965–24970.

[24] S. Bhuvaneswari, P.M. Pratheeksha, S. Anandan, D. Rangappa, R. Gopalan, T. N. Rao, Efficient reduced graphene oxide grafted porous Fe_3O_4 composite as a high-performance anode material for Li-ion batteries, Phys. Chem. Chem. Phys. 11 (2014) 11, https://doi.org/10.1039/C3CP54778G.

[25] V. Gangarajua, B. Da, D. Rangappa, Synthesis and Characterization of α-MoO_3/RGO Composite as anode material for Li-ion batteries using spray drying combustion, Materials Today Proc 4 (2017) 12328–12332.

[26] N. Pal, P. Dubey, P. Gopinath, K. Pal, Combined effect of cellulose nanocrystal and reduced graphene oxide into poly-lactic acid matrix nanocomposite as a scaffold and its anti-bacterial activity, Int. J. Biol. Macromol. 95 (2017) 94–105.

[27] N. Pal, S. Banerjee, P. Roy, K. Pal, Reduced graphene oxide and PEG-grafted TEMPO-oxidized cellulose nanocrystal reinforced poly-lactic acid nanocomposite film for biomedical application, Mater. Sci. Eng. C 104 (2019), 109956.

[28] N. Pal, S. Banerjee, P. Roy, K. Pal, Melt-blending of unmodified and modified cellulose nanocrystals with reduced graphene oxide into PLA matrix for biomedical application, Polym. Adv. Technol. 30 (2019) 3049–3060.

[29] V.S. Amrutha, K.S. Anantharaju, D.S. Prasanna, D. Rangappa, K. Shetty, H. Nagabhushana, K. Ashwini, Y.S. Vidya, G.P. Darshan, Enhanced Sunlight driven photocatalytic performance and visualization of latent fingerprint by green mediated $ZnFe_2O_4$–RGO nanocomposite, Arabian Jour. Chem. 13 (2020) 1449–1465.

[30] M.N. Rani, M. Murthy, N Shyla Shree, S. Ananda, S. Yogesh, D. Rangappa, Cuprous oxide anchored Reduced Graphene oxide ceramic nanocomposite using Tagetes erecta flower extract and evaluation of its antibacterial activity and cytotoxicity, Advanced ceramics and nanomaterials for sustainable development, Ceram. Int. 45 (2019) 25020–25026.

[31] M. Navya Rani, S. Ananda, Dinesh Rangappa, Preparation of reduced graphene oxide and its antibacterial properties, Materials Today Proc 4 (2017) 12300–12305.

[32] Krushitha Shetty, S.V. Lokesh, D. Rangappa, H.P. Nagaswarupa, H. Nagabhushana, K.S. Anantharaju, S.C. Prashantha, Y.S. Vidya, S.C. Sharma, Designing $MgFe_2O_4$ decorated on green mediated reduced graphene oxide sheets showing photocatalytic performance and luminescence property, Physica B 507 (2017) 67–75.

[33] R.M. Zaid, F.C. Chong, E.Y.L. Teo, E.-P. Ng, F. Chong, Reduction of graphene oxide nanosheets by natural beta carotene and its potential use as supercapacitor electrode, Arabian J. Chem. 8 (2014) 560–569.

[34] T. Kuila, S. Bose, P. Khanra, A.K. Mishra, N.H. Kim, J.H. Lee, A green approach for the reduction of graphene oxide by wild carrot root, Carbon 50 (2012) 914–921.

[35] S. Hatamie, O. Akhavan, S.K. Sadrnezhaad, M.M. Ahadian, M.M. Shirolkar, H. Q. Wang, Curcumin-reduced graphene oxide sheets and their effects on human breast cancer cells, Mater. Sci. Eng. C 55 (2015) 482–489.

[36] R.K. Upadhyay, N. Soin, G. Bhattacharya, S. Saha, A. Barman, S.S. Roy, Grape extract assisted green synthesis of reduced graphene oxide for water treatment application, Mater. Lett. 160 (2015) 355–358.

[37] R. Liao, Z. Tang, Y. Lei, B. Guo, Polyphenol-reduced graphene oxide: mechanism and derivatization, J. Phys. Chem. C 115 (2011) 20740–20746.

[38] Y. Wang, Z.X. Shi, J. Yin, Facile synthesis of soluble graphene via a green reduction of graphene oxide in tea solution and its biocomposites, ACS Appl. Mater. Interfaces 3 (2011) 1127–1133.

[39] M. Akhavan, Z. Kalaee, S.A. Ghiasi, A. Esfandiar, Increasing the antioxidant activity of green tea polyphenols in the presence of iron for the reduction of graphene oxide, Carbon 50 (2012) 3015–3025.

[40] B. Haghighi, M.A. Tabrizi, Green-synthesis of reduced graphene oxide nanosheets using rose water and a survey on their characteristics and applications, RSC Adv. 3 (2013) 13365–13371.

[41] B. Kartick, S.K. Srivastava, I. Srivastava, Green synthesis of graphene, J. Nanosci. Nanotechnol. 13 (2013) 4320–4324.

[42] S. Thakur, N. Karak, Green reduction of graphene oxide by aqueous phytoextracts, Carbon 50 (2012) 5331–5339.

[43] D. Suresh, P. Nethravathi, H. Nagabhushana, S. Sharma, Spinach assisted green reduction of graphene oxide and its antioxidant and dye absorption properties, Ceram. Int. 41 (2015) 4810–4813.

[44] U.S. Tayade, A.U. Borse, J.S. Meshram, Green reduction of graphene oxide and its applications in band gap calculation and antioxidant activity, Green Mater. 7 (2019) 1–13.

[45] X. Jin, N. Li, X. Weng, C. Li, Z. Chen, Green reduction of graphene oxide using eucalyptus leaf extract and its application to remove dye, Chemosphere 208 (2018) 417–424.

[46] M. Mahmudzadeh, H. Yari, B. Ramezanzadeh, M. Mahdavian, Urtica dioica extract as a facile green reductant of graphene oxide for UV resistant and corrosion protective polyurethane coating fabrication, J. Ind. Eng. Chem. 78 (2019) 125–136.

[47] K.B. Narayanan, H.D. Kim, S.S. Han, Biocompatibility and hemocompatibility of hydrothermally derived reduced graphene oxide using soluble starch as a reducing agent, Colloids Surf. B Biointerfaces 185 (2020), 110579.

[48] Y. Lei, Z. Tang, R. Liao, B. Guo, Hydrolysable tannin as environmentally friendly reducer and stabilizer for graphene oxide, Green Chem. 13 (2011) 1655–1658.

[49] D. Suresh, M.P. Kumar, H. Nagabhushana, S. Sharma, Cinnamon supported facile green reduction of graphene oxide, its dye elimination and antioxidant activities, Mater. Lett. 151 (2015) 93–95.
[50] Z.-J. Fan, W. Kai, J. Yan, T. Wei, L.-J. Zhi, J. Feng, Y-m. Ren, L.-P. Song, F. Wei, Facile synthesis of graphene nanosheets via Fe reduction of exfoliated graphite oxide, ACS Nano 5 (2011) 191–198.
[51] Z. Fan, K. Wang, T. Wei, J.-Y. Liping, S.B. Shao, An environmentally friendly and efficient route for the reduction of graphene oxide by aluminum powder, Carbon 48 (2010) 1686–1689.
[52] S. Yang, W. Yue, D. Huang, C. Chen, H. Lina, X. Yang, A facile green strategy for rapid reduction of graphene oxide by metallic zinc, RSC Adv. 2 (2012) 8827–8832.
[53] X. Li, X. Xu, F. Xia, L. Bu, H. Qiu, M. Chen, et al., Electrochemically active MnO2/RGO nanocomposites using Mn powder as the reducing agent of GO and the MnO2 precursor, Electrochim. Acta 130 (2014) 305–313.
[54] P. Song, X. Zhang, M. Sun, X. Cui, Y. Lin, Synthesis of graphene nanosheets via oxalic acid-induced chemical reduction of exfoliated graphite oxide, RSC Adv. 2 (2012) 1168–1173.
[55] J. Zhang, H. Yang, G. Shen, P. Cheng, J. Zhang, S. Guo, Reduction of graphene oxide via L-ascorbic acid, Chem. Commun. 46 (2010) 1112–1114.
[56] J. Li, G. Xiao, C. Chen, R. Li, D. Yan, Superior dispersions of reduced graphene oxide synthesized by using gallic acid as a reductant and stabilizer, J. Mater. Chem. 1 (2013) 1481–1487.
[57] M. Mitra, K. Chatterjee, K. Kargupta, S. Ganguly, D. Banerjee, Reduction of graphene oxide through a green and metal-free approach using formic acid, Diam. Relat. Mater. 37 (2013) 74–79.
[58] Z. Bo, X. Shuai, S. Mao, H. Yang, J. Qian, J. Chen, et al., Green preparation of reduced graphene oxide for sensing and energy storage applications, Sci. Rep. 4 (2014) 4684.
[59] M. Seo, D. Yoon, K.S. Hwang, J.W. Kang, J. Kim, Supercritical alcohols as solvents and reducing agents for the synthesis of reduced graphene oxide, Carbon 64 (2013) 207–218.
[60] H. Peng, L. Meng, L. Niu, Q. Lu, Simultaneous reduction and surface functionalization of graphene oxide by natural cellulose with the assistance of the ionic liquid, J. Phys. Chem. C 116 (2012) 16294–16299.
[61] C. Zhu, S. Guo, Y. Fang, S. Dong, Reducing sugar: new functional molecules for the green synthesis of graphene nanosheets, ACS Nano 4 (2010) 2429–2437.
[62] O.G. Akhavan, E. Ghaderi, Escherichia coli bacteria reduce graphene oxide to bactericidal graphene in a self-limiting manner, Carbon 50 (2012) 1853–1860.
[63] S. Gurunathan, J.W. Han, J.H. Park, V. Eppakayala, J.-H. Kim, Ginkgo biloba: a natural reducing agent for the synthesis of cytocompatible graphene, Int. J. Nanomed. 9 (2014) 363.
[64] G. Wang, F. Qian, C.W. Saltikov, Y. Jiao, Y. Li, Microbial reduction of graphene oxide by Shewanella, Nano Res 4 (2011) 563–570.
[65] M. Fernandez-Merino, L. Guardia, J. Paredes, S. Villar-Rodil, P. Solis-Fernandez, A. Martinez-Alonso, et al., Vitamin C is an ideal substitute for hydrazine in the reduction of graphene oxide suspensions, J. Phys. Chem. C 114 (2010) 6426–6432.
[66] J. Gao, F. Liu, Y. Liu, N. Ma, Z. Wang, X. Zhang, Environment-friendly method to produce graphene that employs vitamin C and amino acid, Chem. Mater. 22 (2010) 2213–2218.
[67] P. Khanra, T. Kuila, N.H. Kim, S.H. Bae, D.-S. Yu, J.H. Lee, Simultaneous bio-functionalization and reduction of graphene oxide by baker's yeast, Chem. Eng. J. 183 (2012) 526–533.
[68] X. Fan, W. Peng, Y. Li, X. Li, S. Wang, G. Zhang, F. Zhang, Deoxygenation of exfoliated graphite oxide under alkaline conditions: a green route to graphene preparation, Adv. Mater. 20 (2008) 4490–4493.
[69] Y. Jin, S. Huang, M. Zhang, M. Jia, D. Hu, A green and efficient method to produce graphene for electrochemical capacitors from graphene oxide using sodium carbonate as a reducing agent, Appl. Surf. Sci. 268 (2013) 541–546.
[70] X. Zhang, K. Li, H. Li, J. Lu, Q. Fu, Y. Chu, Graphene nanosheets synthesis via chemical reduction of graphene oxide using sodium acetate trihydrate solution, Synth. Met. 193 (2014) 132–138.
[71] M.T.H. Aunkor, I.M. Mahbubul, R. Saidurb, H.S.C. Metselaar, The green reduction of graphene oxide, RSC Adv. 6 (2016) 27807.
[72] Priya Srivastava, P. Kumar, D.K. Singh, V.K. Singh, Biological properties of thuja orientalis linn, Adv. Life Sci. 2 (2012) 17–20.
[73] K.M. Hold, N.S. Sirisoma, T. Ikeda, T. Narahashi, J.E. casida, Alpha-thujone (the active component of absinthe): gamma-aminobutyric acid type A receptor modulation and metabolic detoxification", Proc. Natl. Acad. Sci. U.S.A. 97 (2000) 3826–3831.
[74] R. Biswas, S.K. Mandal, S. Dutta, S.S. Bhattacharyya, N. Bou-jedaini, A.R. Khuda-Bukhsh, Thujone-rich fraction of thuja occidentalis demonstrates major anti-cancer potentials: evidences from in vitro studies on A375 Cells, Evid-Based Compl Alt (2011) 16, https://doi.org/10.1093/ecam/neq042. Article ID 568148.
[75] K. Shimada, Contribution to anatomy of the central nervous system of the Japanese upon the vermal arbour vitae, Okajimas Folia Anat. Jpn. 28 (1956) 207–227.
[76] D. Baran, Arbor vitae, A guarantee of health, revista medico-chirurgicala a societatii de medici si naturalisti din lasi 95 (1991) 347–349.
[77] S.K. Dubey, A. Batra, Antioxidant activity of thuja occidentalis linn, Asian J. Pharmaceut. Clin. Res. 2 (2009) 73–76.
[78] S.K. Dubey, A. Batra, Hepatoprotective activity from ethanol fraction of Thuja occidentalis Linn, Asian J. Res. Chem. 1 (2008) 32–35.
[79] Jiaqi Huang, J. Stephanie, Weinstein, Kai Yu, Satu Männistö, Demetrius albanes relationship between serum Alpha-Tocopherol and overall and cause-specific mortality: a 30-year prospective cohort analysis, Circ. Res. 125 (2019) 29–40.
[80] R. Yamauchi, Vitamin E: mechanism of its antioxidant activity, Food Sci. Technol. Int. Tokyo 3 (1997) 301–309.
[81] A. Kontush, S. Meyer, B. Finckh, A. Kohlschütter, U. Beisiegel, α-Tocopherol as a reductant for Cu (II) in human lipoproteins: triggering role in the initiation of lipoprotein oxidation, J. Biol. Chem. 271 (1996) 11106–11112.
[82] E. Choe, D.B. Min, Mechanisms of antioxidants in the oxidation of foods, Comprehen. Rev. Food Sci. and Food Safety 8 (2009) 345–388.
[83] S.B. Nimse, D. Pal, Free radicals, natural antioxidants, and their reaction mechanisms, RSC Adv. 5 (2015) 27986.
[84] H.B. Shao, L.-Y. Chu, Z.-H. Lu, C.-M. Kang, Primary antioxidant free radical scavenging and redox signaling pathways in higher plant cells, Int. J. Biol. Sci. 4 (2008) 8–14.
[85] J.M. Tucker, D.M. Townsend, Alpha-tocopherol: roles in prevention and therapy of human disease, Biomed. Pharmacother. 59 (2005) 380–387.
[86] L. García-Hernández, D. Arenas-Islas, P.A. Ramírez-Ortega, M.U. Flores-Guerrero, D. Neri-Enriquez, Green synthesis, characterization and stabilization of nanoparticles silver with thuja orientalis extract, J Nanomater. Mol. Nanotechnol. 5 (2016) 5.
[87] A. Bandyopadhyay, P.P. Banerjee, P. Shaw, M.K. Mondal, V.K. Das, P. Chowdhury, N. Karak, S. Bhattacharya, A. Chattopadhyay, Cytotoxic and mutagenic effects of thuja occidentalis mediated silver nanoparticles on human peripheral blood lymphocytes, Mater. Focus 6 (2017) 290–296.
[88] V. Stengl, J. Henych, J. Bludská, P. Ecorchard, M. Kormunda, A green method of graphene preparation in an alkaline environment, Ultrason. Sonochem. 24 (2015) 65–71.
[89] W. Gao, L.B. Alemany, L. Ci, P.M. Ajayan, New insights into the structure and reduction of graphite oxide, Nat. Chem. 1 (2009) 403–408.
[90] S.C. Chelgani, M. Rudolph, R. Kratzsch, D. Sandmann, J. Gutzmer, A review of graphite beneficiation techniques, Miner. Process. Extr. Metall. Rev. 37 (2016) 58–68.
[91] S. Some, P. Bhunia, E. Hwang, K. Lee, Y. Yoon, S. Seo, H. Lee, Can commonly used hydrazine produce n-type graphene? Chem. Eur J. 18 (2012) 7665–7670.
[92] C.H. Lui, T.F. Heinz, Measurement of layer breathing mode vibrations in few-layer graphene, Phys. Rev. B 87 (2013), 121404.
[93] Q. Zheng, B. Zhang, X. Lin, X. Shen, N. Yousefi, Z. Huang, Z. Li, J. Kim, Highly transparent and conducting ultra large graphene oxide/single-walled carbon nanotube hybrid films produced by Langmuir–Blodgett assembly, J. Mater. Chem. 22 (2012) 25072.
[94] G. Eda, M. Chhowalla, Chemically derived graphene oxide: towards large-area thin-film electronics and optoelectronics, Adv. Mater. 22 (2010) 2392–2415.
[95] W. Ai, L. Xie, Z. Du, Z. Zemg, J. Liu, H. Zhnag, Y. Hunag, W. Hunag, T. Yu, A novel graphene-polysulfide anode material for high-performance lithium-ion batteries, Sci. Rep. 3 (2013) 2341.
[96] L. Ren, K.N. Hui, K.S. Hui, Y. Liu, X. Qi, J. Zhong, Y. Du, J. Yang, 3D hierarchical porous graphene aerogel with tunable meso-pores on graphene nanosheets for high-performance energy storage, Sci. Rep. 5 (2015) 14229.
[97] S.J. Qiao, X.N. Xu, Y. Qiu, H.C. Xiao, Y.F. Zhu, Simultaneous reduction and functionalization of graphene oxide by 4-hydrazinobenzenesulfonic acid for polymer nanocomposites, Nanomaterials 6 (2016) 29.
[98] S. Some, Y. Kim, Y. Yoon, H. Yoo, S. Lee, Y. Park, H. Lee, High-quality reduced graphene oxide by a dual-function chemical reduction and healing process, Sci. Rep. 3 (2013) 1929.
[99] S.K. Pradhan, B. Xiao, S. Mishra, A. Killam, A.K. Pradhan, Resistive switching behavior of reduced graphene oxide memory cells for low power nonvolatile device application, Sci. Rep. 6 (2016) 26763.
[100] C. Mattevi, G. Eda, S. Agnoli, S. Miller, K.A. Mkhoyan, O. Celik, D. Mastrogiovanni, G. Granozzi, E. Garfunkel, M. Chhowalla, Evolution of electrical, chemical, and structural properties of transparent and conducting chemically derived graphene thin films, Adv. Funct. Mater. 19 (2009) 2577–2583.
[101] S.V. Jovanovic, S. Steenken, Y. Hara, M.G. Simic, Reduction potentials of flavonoid and model phenoxyl radicals. Which ring in flavonoids is responsible for antioxidant activity? J. Chem. Soc, Perkin. Trans. 2 (1996) 2497–2504.
[102] E. Choe, D.B. Min, Chemistry and reactions of reactive oxygen species in foods, J. Food Sci. 70 (2005) 142–159.
[103] E.H. Lee, D.G. Song, J.Y. Lee, C.H. Pan, B.H. Um, S.H. Jung, Flavonoids from the leaves of Thuja orientalis inhibit the aldose reductase and the formation of advanced glycation endproducts, J. Korean Soc. Appl. Biol. Chem. 52 (2009) 448–455.
[104] U. Takahama, S. Hirota, Possible reactions of dietary phenolic compounds with salivary nitrite and thiocyanate in the stomach, Antioxidants 6 (2017) 53.
[105] O. Makhotkina, P.A. Kilmartin, Uncovering the influence of antioxidants on polyphenol oxidation in wines using an electrochemical method: cyclic voltammetry, J. Electroanal. Chem. 633 (2009) 165–174.
[106] V. Georgakilas, J.N. Tiwari, K.C. Kemp, J.A. Perman, A.B. Bourlinos, K.S. Kim, R. Zboril, Noncovalent functionalization of graphene and graphene oxide for energy materials, biosensing, catalytic, and biomedical applications, Chem. Rev. 116 (2016) 5464–5519.

[107] M. Noruzi, M. Mousivand, Instantaneous green synthesis of zerovalent iron nanoparticles by Thuja orientalis extract and investigation of their antibacterial properties, J. Appl. Chem. Res. 9 (2015) 37–50.
[108] M. Th Al-Azawi, S.M. Hadi, Ch H. Mohammed, Synthesis of silica nanoparticles via green approach by using hot aqueous extract of thuja orientalis leaf and their effect on biofilm formation, Iraqi J. Agric. Sci. 50 (2019) 245–255.
[109] N. Tz Dintcheva, R. Arrigo, C. Gambarotti, S. Carroccio, G. Filippone, F. Cicogna, M. Guenzi, α-Tocopherol-induced radical scavenging activity in carbon nanotubes for thermo-oxidation resistant ultra-high molecular weight polyethylene-based nanocomposites, Carbon 74 (2014) 14–21.